Protein adsorption and activity on carbon xerogels with narrow pore size distributions covering a wide mesoporous range

LUIS A. RAMÍREZ-MONTOYA, ALEJANDRO CONCHESO, ISABEL D. ALONSO-BUENAPOSADA, HÉCTOR GARCÍA, J. ÁNGEL MENÉNDEZ, ANA ARENILLAS, MIGUEL A. MONTES-MORÁN*

Instituto Nacional del Carbón, INCAR-CSIC, Apartado 73, 33080 Oviedo, Spain

* Corresponding author phone: +34 985118996; fax: +34 985299076; e-mail: miguel.montes@csic.es (Miguel Montes-Morán)

Abstract

Four carbon xerogels (CXs) were used to study the effect of the average pore size (APS) on the adsorption and activity of cytochrome c (cyt c). Pore size distributions of the CXs were relatively narrow with APSs covering the whole mesoporosity range (5, 15, 30 and 55 nm), as determined by mercury porosimetry. Selected techniques verified that all carbons were identical in terms of composition and surface chemistry. The best APS for cyt c adsorption (in terms of capacity) was 30 nm, with loadings of 180 mg of protein (g of support)$^{-1}$. The CX with APS of 15 nm also hosted high amounts of cyt c, followed by the material with 55 nm. The CX with 5 nm APS did not adsorb cyt c. The pH of adsorption had little effect on the final amount adsorbed, thus stressing the hydrophobic nature of the protein/carbon surface interaction. The activity of the resulting materials towards the ABTS oxidation was similar regardless the amount of cyt c adsorbed on their surface/pores. Their performance in successive cycles of re-use was different depending on the carbon support; xerogels bearing APSs ≥ 15 nm presented an increasing activity with increasing the number of cycles.

1. Introduction

The interaction of proteins with porous substrates is crucial for a number of applications [1,2]. It is however appalling the little role that porous carbons play in this area. A possible explanation might be linked to the scientific and technical interest of the carbon community being traditionally focused on the production of (microporous) activated carbons [3]. Due to the size of most biomolecules of interest, microporosity seems not relevant [3,4]. This situation could be reverted as an increasing interest on protein/porous carbons systems is steadily shown [5,6]. Actually, it was the development of the so-called nanostructured mesoporous carbons [7-9] what steered the scientific research on this particular issue [10-13]. Still, studies on mesoporous carbons are few compared to those carried out on mesoporous silicates or aluminosilicates [14-19], in spite of the well-known strengths of the carbon supports [20,21].

Nevertheless, most studies on the interaction of proteins with mesoporous materials concentrate in a rather narrow range, normally below 20 nm of average pore size. These pore sizes are well below those used in commercial supports (> 50 nm) and there are already studies questioning the suitability of nanostructured mesoporous materials to support proteins for real applications [22-24]. The debate on the effect of pore size on the performance of supported proteins is still far from conclusion due to two different factors. First, there is a lack of studies that evaluate the adsorption of biomolecules on similar supports with pore size distributions (PSDs) covering wider ranges of average pore sizes. Second, most studies focus only on the adsorption process rather than also accounting for the activity of the supported enzymes. The possibility of using a set of carbon materials to evaluate the effect of the pore size on the adsorption and activity of the resulting materials is not straightforward. It should be

pointed out here that, due to the sensibility of the protein activity to the surroundings, changes on the surface chemistry or composition of the carbon materials could hinder the effect of their different textural properties [21,22].

Carbon xerogels obtained by the carbonisation of resorcinol (R)/formaldehyde (F) organic gels could be ideal candidates for this purpose [25]. Specifically, it has been demonstrated that the macro and mesoporosity of the carbon xerogels mimics those of the RF organic xerogels, which in turn can be tuned precisely over the entire nanoscale (from 2 nm to 1000 nm) by controlling a number of variables during their synthesis [26]. Microwave heating can be used to speed up the gelation and curing processes of the RF sols, thus lowering costs. Carbon materials resulting from the carbonisation of the RF organic xerogels are highly reproducible solids of very high purity, with negligible ash contents [27].

This work studies the effect of the pore size on the protein loading and activity using four carbon xerogels with relatively narrow PSD. The maxima of such PSD cover the whole range of mesoporosity (from 5 nm to 55 nm). Cytochrome c (cyt c) has been selected as a protein model due to the high purity of the product commercially available, its use in other immobilisation studies [19], and the deep knowledge of its structure and physicochemical properties [18]. Factors that are known to affect the adsorption process and the activity of the supported cyt c have been considered.

2. Experimental

2.1. Synthesis of the carbon xerogels

Four different carbon xerogels (CXs) were prepared for this study by using a method reported previously [25,26]. Essentially, organic xerogels were first synthesised by the

polycondensation of resorcinol (Indspec, 99.6% purity) and formaldehyde (Merck, 37% aqueous solution, including 0.7 % methanol) (RF) in deionised water and methanol (VWR Chemicals, Normapur >99.9 % purity) using selected conditions (see below). A lab-made microwave device was set to heat the solutions up to 85 ºC for 3 h. Excess water was afterwards eliminated by continuing to heat the gel in the microwave oven until a mass loss of over 50% of the initial weight was achieved. Finally, organic xerogels were converted into CXs by heating them (25 g) in a quartz reactor (i.d. 30 mm) placed in a horizontal electrical tube furnace (Carbolite Type MFT 12/38/400), under a nitrogen flow rate of 100 ml min^{-1} up to 700 ºC at 50 ºC min^{-1} and 2 h dwell time. The carbonised RF carbon xerogel particles were cooled down to room temperature under the same nitrogen flow rate. Carbon xerogels were finally milled and sieved down to 1-2 mm particles.

Following previous studies, four variables related to the RF solutions are known to affect the porosity of the organic xerogels OXs (hence of the carbon xerogels CXs). These variables include the R/F ratio, the dilution ratio D (defined as the molar ratio between the total solvent and reactants, see [25]), the pH of the sol and the amount of MeOH contained in the formaldehyde solution (MeOH %). Table 1 gives the values of each variable for the different supports.

2.2. Characterisation of the carbon xerogels

N_2 adsorption-desorption isotherms were performed at -196 ºC in a Micromeritics Tristar II volumetric adsorption system. Prior to measurement, samples were outgassed by heating overnight at 120 ºC under vacuum. The Brunauer–Emmett–Teller and Dubinin-Radushkevich models were selected to determine the BET surface area and micropore volume of the CXs from the nitrogen adsorption data, respectively.

The true density of the CXs (ρ_{He}) was measured with a Micromeritics AccuPyc 1330 pycnometer, using helium as the probe gas. The samples were outgassed at 120 °C overnight prior to analysis. The apparent density (ρ_{Hg}) was determined with mercury on a Micromeritics AutoPore IV apparatus. The samples were also outgassed at 120 °C overnight. The pore volume distributions were evaluated with a mercury porosimeter with a maximum operating pressure of 227 MPa. The percentage of open porosity (s) was calculated as:

$$s = [1-(\rho_{Hg}/\rho_{He})] \times 100 \quad (1)$$

Elemental analysis of the samples was carried out in LECO apparatuses (LECO CHNS-932 and LECO VTF-900 to determine the oxygen content). The characterisation of the surface chemistry of the CXs included the determination of their point of zero charge (pH_{PZC}) [28], as well as XPS and TPD analyses. XPS measurements were carried out in a SPECS Phoibos 100 analyser using MgKα X-rays (1253.6 eV) at a power of 120 W and in a residual vacuum of 10^{-7} Pa. Measurements were made with the analyser in fixed transmission mode and normal to the plane of the sample. Analyser pass energy of 80 eV was used to collect broad scan spectra (0–1100 eV). The atomic percentages (atom %) of the different elements present in the approx. 10 nm upper layer probed by XPS were calculated from the survey spectra by considering the integrated areas of the main XPS peaks. Representative amounts (around 100 mg) of the CXs were tested. Typical standard deviation of the measurements is within ±0.5 atom% of the reported values. C (1s) high resolution spectra were obtained using a pass energy of 25 eV. Peaks were deconvoluted fitting Gaussian-Lorentzian functions by means of CasaXPS software. Peak assignment was carried out following previous studies [29,30].

For TPD experiments, ca. 20 mg of the CXs were heated at 10 ºC min^{-1} under a He flow of 50 ml min^{-1} in the quartz reactor of an Autochem II apparatus (Micromeritics). Desorbed gases were analysed using an Omnistar (Pfeiffer Vacuum) mass spectrometer. TPD curves were obtained by plotting the desorbed CO and CO_2 (µmol g^{-1} s^{-1}) vs. the temperature (ºC). TPD curves were deconvoluted using homemade software, following the criteria reported in previous studies [31,32].

2.3. Immobilisation of biomolecules

Cytochrome c (cyt c) from bovine heart (Sigma-Aldrich, ref C2037) was selected for the immobilisation experiments due to its high purity (≥ 95%; 12327 Da). Solutions of cyt c (0.5 g L^{-1}) were prepared in different pH buffers: phosphoric acid/sodium phosphate (pH 3), sodium phosphate (pH 6) and sodium carbonate (pH 10). The total ionic strength of all buffer solutions was set to 100 mM. CXs particles of 1-2 mm in size were suspended in the buffer solutions 24 h prior their use as biomolecules supports. In a typical immobilisation experiment, 10 mg of a CX were suspended in 5 mL of the cyt c solution prepared in the selected buffer. This was done in screw top vials that were then orbitally shaken at 200 rpm and kept at 30 ºC in an incubator shaker (TH 15 model form Edmund Bühler GmbH)) for up to 96 h. Aliquots were periodically withdrawn from the supernatant solution to quantify the cyt c content remaining in the liquid phase. Quantification of the cyt c in the solutions was performed by UV-vis spectrometry (Shimadzu UV-2401 PC scanning spectrophotometer). Absorbances at ca. 410 nm ($\varepsilon = 10^5$ M^{-1} cm^{-1}) were used to determine the concentration of cyt c in a given solution. In addition, Bio-Rad protein assays (Bio-Rad Labs, ref. 500-0002) were carried out to determine the amount of protein present in the initial and final (equilibrium) solutions [33]. This protein quantification methodology is a standard procedure that was performed on separate experiments after 24 h and 96 h of immobilisation time. At least, duplicates of each immobilisation experiment were carried out simultaneously to attain statistical soundness. Also, blank tests (i.e., cyt c solutions

without carbon supports) were also performed in order to test the stability of the proteins under the immobilisation test conditions. Once prepared, the resulting solids were maintained in buffer suspensions (pH 6) inside a refrigerator (4 ºC) for further use.

2.4. Activity assays

Cytochrome c, which is known to present peroxidic activity, was tested on the oxidation of 2,2'-Azino-bis(3-ethylbenzthiazoline-6-sulfonic acid) diammonium salt (ABTS^{TM}) (Sigma-Aldrich, ≥ 98% HPLC) by following spectrophotometrically the absorbance of the band at 420 nm (ε = 36000 M^{-1} cm^{-1}) [32-34]. Unsupported protein assays were carried out with cyt c solutions (0.5 g L^{-1}) in pH 3, 6 and 10 buffers (see above). ABTS solutions (1 mM) were prepared in buffers covering a wider pH interval, from 2-10 (pH 2 and 3 buffers: phosphoric acid/sodium phosphate; pH 4 and 5 buffers: sodium acetate; pH 6, 7 and 8 buffers: sodium phosphate; and pH 10 buffer: sodium carbonate; all 100 mM total ionic strength buffers). Equal amounts (1.9 mL) of the ABTS (1 mM) and H_2O_2 (VWR Chemicals, Normapur, about 30 %) (10 mM) solutions buffered at pH 4 (100 mM total ionic strength) were mixed in a UV cuvette. 0.2 mL of the cyt c solution was finally added to sum a total reaction volume of 4 mL. The change in the absorbance at 420 nm was measured continuously. The activity of the unsupported cyt c was calculated from the slope of the linear part of the absorbance vs. time plot. One unit of cyt c activity (U) is defined as the amount of protein that oxidises 1 µmol of ABTS to coloured products per minute. At least, two experiments under the same conditions were carried out.

In the case of the cyt c supported on the carbon xerogels, 10 mg of the solid particles loaded with cyt c (see Section 2.3) were suspended, at a controlled time, in screw top vials containing a mixture of 5 mL of ABTS (1 mM, pH 4 buffer) and 5 mL of H_2O_2 (10 mM, pH 4 buffer) (i.e., total volume of reaction = 10 mL). Aliquots of the supernatant

solution were extracted at selected times to measure the absorbance at 420 nm. After measuring, volumes were returned to the original solution. At least 6 points (i.e., 6 extractions) were carried out in every activity assay. The activity of the cyt c/CX materials was then calculated from the slope of the absorbance vs. time plot. A minimum of two experiments were run in parallel for each activity test.

The reusability of the materials was evaluated by measuring the change in activity after successive cycles of reaction using ABTS as substrate. Both ABTS and H_2O_2 solutions were replaced in each cycle, which was carried out until complete ABTS oxidation. Two successive washes of the biocatalysts were performed under vortex shaking (30 Hz) for 5 min in 5 mL pH 6 buffer (100 mM) before each cycle.

3. Results and discussion

3.1. Carbon xerogels characteristics

Figure 1 shows the nitrogen isotherms of the four CXs synthesised in this study. They are all type IV isotherms, which are characteristic of mesoporous materials. The hysteresis loop of samples CX-15, 30 and 55 is very similar, with a sharp decrease of the desorption branch (H1 hysteresis loop type) at p/p_0 values well over 0.8. The hysteresis loop of the CX-55 sample is hardly perceptible, which indicates that mesopores in this sample are too wide to be detected by N_2 adsorption. On the other hand, the hysteresis loop closing point gradually moves to lower p/p_0 values from CX-55 to CX-5, suggesting a decrease of the average mesopore size of those samples. The desorption hysteresis in the isotherm of sample CX-5 is however much less steeper resembling a H4 loop-type. This denotes a wider distribution of mesopores for this particular carbon xerogel. Selected textural parameters obtained (or calculated) from the adsorption isotherms are presented in Table 2. As expected from the

isotherms (Figure 1), the micropore volumes (V_{DR}) of all samples are almost identical. Hence, since the BET surface area is mainly controlled by their microporosity, the S_{BET} values of the CXs are very similar.

Due to the mesoporous nature of the CXs under study, Hg intrusion was considered a more adequate technique than N_2 adsorption at -196 ºC to ascertain the pore size distributions of the samples (Figure S1 and Figure 2). The mercury pore size distributions of Figure 2 reflect the versatility of the here reported route for the preparation of designed carbon xerogels. Thus, relatively narrow pore size distributions were obtained for the CX-55, CX-30 and, especially, CX-15. The maximum of those distributions (in nm) were used for sample labelling, i.e., CX-30 corresponds to the carbon xerogel having a pore size distribution with a maximum centred at ca. 30 nm. The pore size distribution of the CX-5 sample reaches the lower limit of the technique (5.5 nm, Figure 2). Still, assuming a curve with a normal distribution shape (similar to those obtained for the rest of carbon xerogels), it seems that the maximum of the mesopore size distribution would be located near 5 nm (see inset in Figure 2). A DFT pore size distribution derived from the nitrogen isotherm of this particular sample would corroborate this (Figure S2), although, as expected from the shape of the isotherm (Figure 1), the N_2 PSD of CX-5 (Figure S2) is wider than that of Hg intrusion (Figure 2). The volume of the pores with sizes comprised within the Hg PSD of Figure 2 was also calculated for CX-15, -30 and -55. Results are included in Table 2. For CX-15, the mesopore volume estimation from N_2 adsorption isotherms agrees very well with the pore volume calculated from Hg intrusion. Those pore volumes start to deviate as the PSD moves to higher values (CX-30). For CX-55, such comparison makes little sense since the maximum of the Hg PSD is located in the macropore region (Figure 2).

The different synthesis conditions of the organic xerogels counterparts brought about materials with RF condensed clusters increasing in size and/or having higher inter-

cluster distances from CX-5 to CX-55 [35]. As a consequence, the apparent density (ρ_{Hg}) of the carbon xerogels decreases from CX-5 to CX-55 (Table 2). Since the true density (ρ_{He}) is very similar for all the carbons, the percentage of open porosity differs strongly from CX-5 to CX-55 (Table 2).

As for the chemical properties, all techniques rendered similar, if not identical results for all CXs. Thus, starting with the elemental analysis results, all materials were mainly composed of carbon (approx. 95 % for all samples), with small amounts of oxygen (ranging from 3-3.5 %) and hydrogen (1.5 % for all samples). The pH_{PZC} of all carbons was around 8.5.

XPS analyses also showed very similar compositions on the surface of all carbon xerogels (Table 3). Differences in C and O atom% on three of the carbon supports (CX-15, -30 and -55) are within the experimental error of the technique. CX-5 seems to have a slightly higher oxygen concentration on its surface than the rest of CXs. In spite of such a rather low surface oxygen concentration, carbon chemical bonding environment information was obtained by measuring C1s high resolution XPS profiles of the carbon xerogels. They were found to be almost identical for all samples (Figure 3). Figure S3 shows the deconvolution of one of those C1s profiles (that of CX-5), where contributions from C-OR (R including H), C=O and O=C-OR (R including H) were included at +1.5, +2.6 and +4.5 eV of the C(sp^2) peak at 284.4 eV, respectively. The last contribution (O=C-OR) which amounts for ca. 5% of the total C1s area is possibly overestimated since it exhibits a rather higher peak width (FWHM) than the rest of contributions.

TPD analyses were also carried out. The CO and CO_2 profiles of all carbons are shown in Figure 4. The total amounts of CO and CO_2 obtained by integration of the emission profiles for the different carbon xerogels are also collected in Table 3. Values are again

very similar between samples. They are very low when compared with the emissions measured for other carbon materials, including activated carbons [30]. Figure S4 shows the deconvolution of the CO and CO_2 profiles of CX-55, which is representative for the rest of them. In the case of the CO TPD profile, five different peaks were selected to contribute to the overall signal. The two peaks at temperatures below 400 ºC are more likely related to the decomposition of carbonyl groups in ketones and aldehydes [30,36]. The three peaks contributing to the maximum CO emission signal (> 400 ºC) are normally ascribed to the decomposition of carboxylic anhydrides (600-610 ºC), phenols (ca. 730 ºC) and carbonyl/quinones (ca. 830 ºC). Analysis of the CO_2 emission signal included four peaks, the main one at 250 ºC corresponding to strongly acidic carboxylic groups. The peaks at approx. 400, 550 and 740 ºC are normally assigned to the decomposition of less acidic carboxylic groups, carboxylic anhydrides and lactones, respectively [30].

In summary, the characterisation of the CXs points out that they differ in their textural properties, i.e., mesopore size distribution and mesopore volumes, but do not differ on their surface properties. The surface chemistry of the supports should be considered almost identical. Minor differences should be attributed to the carbonisation process rather than to the synthesis of the organic xerogels. Therefore, eventual differences in the cyt c adsorption capacities of the CXs and/or the activity of the immobilised cyt c should be ascribed to differences in the textural properties of the carbon supports.

3.2. Immobilisation of Cytochrome c on the carbon xerogels

The adsorption of biomolecules on porous supports could be affected by a number of factors including ionic strength, particle size, temperature, shaking conditions and pH. In order to minimise the number of influencing factors and to concentrate on the effect of pore size of the carbon xerogels, preliminary tests were carried out to fix some of the experimental conditions for the immobilisation tests. Accordingly, ionic strength,

temperature, shaking, cyt c concentration, mass of the support/solution volume ratio and particle size were set for all immobilisation experiments, as detailed in Section 2.3. Only the influence of the pH of the cyt c solution on the performance of the supports was thus considered.

Figure 5 shows the capacities of the different supports when using cyt c solutions (0.5 g L^{-1}) in three different buffers (pH 3, pH 6 and pH 10). The protein loadings reported in Figure 5 were measured after 24 and 96 h of immersion of the CXs particles in the cyt c solutions. Both values are spectroscopic determinations, i.e., calculated from the absorbance of the supernatant liquid at 410 nm. Protein uptake values measured by using the Bio-Rad method were found to match the spectroscopic determination (both at 24 h and 96 h, Figure S5), within experimental error. The adsorption experiments were carried out up to 96 h in most cases due to practical considerations, i.e., the increase on the support capacities at higher times of exposure was very low (less than 5 % of the values at 96 h) as tested randomly using some of the carbon xerogels. It should be also noted that the stability of pH 10 unsupported cyt c solutions is compromised beyond 96 h, under the experimental conditions of adsorption used.

Results of Figure 5 indicate that cyt c is hardly adsorbed at all in CX-5, with capacities well below 10 mg g^{-1}. For this particular support, immobilisation time was extended up to 144 h at pH 6, but the amount adsorbed was virtually the same. In this case, pores of 5 nm seem too tight to host cyt c (4 nm of spherical diameter) [18]. Results obtained on the immobilisation of cyt c on nanostructured mesoporous carbons would contradict this finding. Thus, values as high as ca. 230 mg g^{-1} were obtained on a CMK-3 mesoporous carbon with an average pore size of 4.5 nm [10]. However, a closer inspection of the results reported in that work reveals that such high values were obtained when using solutions with a very high cyt c concentration (4 g L^{-1}). The capacity of the same support when using 0.5 g L^{-1} solutions of is lower, between 150-

190 mg g^{-1}. Those values are still more than an order of magnitude higher than the loadings of CX-5. Cyt c loadings on mesoporous silica with average pore sizes around 5 nm are in the 40-80 mg g^{-1} interval [15,18], albeit the pioneering work of Balkus Jr. group [16] reports loadings very similar to ours (6-10 mg g^{-1}). It should be clear that one main difference in our adsorption studies with respect to the use of nanostructured mesoporous systems is the particle size of the supports, i.e., tens of microns in the case of nanostructured mesoporous carbons or silicas vs. 1-2 mm for the CXs used in this work (see Experimental Section). Particle size and even particle shape are known to affect strongly the adsorption of biomolecules [37]. Furthermore, compared with carbon xerogels, the diffusion of the biomolecules in ordered mesoporous carbons would be enhanced by elimination of pore tortuosity. The straight mesoporous channels present in those ordered mesoporous carbons would facilitate the diffusion of the molecules and, therefore, could increase the adsorption capacity of the support.

The maximum capacities (at 96 h) were attained when using the CX-30 carbon xerogel in the three different pH environments; next comes CX-15 and, finally, CX-55. Although the adsorption studies on carbon materials with average pore sizes > 30 nm are very scarce, Vijayaraj et al. found capacities of less than 10 mg g^{-1} for a series of nanostructured carbon materials with average pore sizes of 30, 50 and 150 nm [38], much lower thus than the capacities of the CX-30 and CX-55 (Figure 5). As just mentioned in the case of CX-5, the immobilisation conditions, particularly the particle size and pore geometry, might be crucial to understand the differences between the capacities of CXs and the supports of [38].

Since the CXs differ not only in their average pore size but also in the pore volume, protein adsorption results expressed in a volumetric basis are relevant (Table 4). Pore volumes calculated from Hg intrusion (V_{Hg}, Table 2) were selected for such calculations for all supports but CX-5, for which the mesopore volume estimation from the N_2

isotherm was used (V_{meso}, Table 2). An alternative, more intuitive way of depicting the influence of the different pore volumes of the supports is the calculation of the pore filling percentages. An estimation of the cyt c density can be drawn from the protein volume and its molecular mass [39,18]. Thus, taking values of the unit cell of the horse heart cyt c (and assuming that they are essentially the same for the bovine heart cyt c used here) [39], a density of 0.17 g cm^{-3} results. Pore filling percentages can be thus estimated for the different carbon xerogels (Table 4, values in parentheses). These new values indicate that not only CX-30 but also CX-15 are very effective supports for cyt c hosting in terms of pore filling, with values ≥ 75 % for the three pH conditions. The porosity of CX-55, on the other hand, is only partially filled by cyt c.

Results of Figure 5 do not show a clear effect of the pH of the cyt c buffer solution on the final protein uptakes of the carbon xerogels. In any case, the maximum adsorption capacities are not happening at pHs close to the isoelectric point of cyt c (pI = 10.5). This finding contradicts previous results of different proteins adsorption on nanostructured mesoporous carbons [10,11,40]. The little effect of the solution pH on the final cytc loading on the CXs suggests that electrostatic interactions are not playing a significant role in the adsorption in this particular biomolecule/support system. If electrostatic interactions were governing the adsorption, in accordance with the cyt c isoelectric point and the carbon xerogels pH_{PZC} (ca. 8.5), maximum and minimum protein loadings would be expected at pH 10 and pH 3, respectively, which is not the case (Figure 5). At pH 10, the solid surface is negatively charged whereas the cyt c molecules are positively charged. On the other hand, at pH 3, both CXs surface and cyt c molecules would be positively charged. The irrelevance of the electrostatic interactions here might be understood in terms of the high carbon content of the carbon xerogels or, alternatively, the lack of a rich surface chemistry despite of its basic character [41]. For these particular materials, protein/carbon surface hydrophobic interactions would control the adsorption process. Such hydrophobic interactions are

known to be strongly affected by the total ionic strength of the protein solution, the higher the ionic strength the higher the level of interaction [42]. To confirm this hypothesis, further immobilisation experiments were carried out on the CX-15 carbon xerogel using cyt c dissolved in a pH 3 phosphoric acid-sodium phosphate buffer of 1 mM ionic strength. The amount adsorbed at 96 h decreased dramatically from 111 mg g^{-1} (100 mM, Figure 5) to 36 mg g^{-1} (1 mM). A similar effect has been reported for the adsorption of cyt c on a nanostructured organosilicate [18]. In any case, this very same argument should be valid for the adsorption of cyt c on nanostructured mesoporous carbons, since they are virtually pure carbon materials with hydrophobic surfaces [8,9,13]. The maximum loadings obtained on those materials when working with solutions pH near the isoelectric point of the proteins is ascribed to the effective molecular diameter of the adsorbate [10,11]. Thus, charged biomolecules would experience adsorbate-adsorbate repulsive forces that would reduce the amount of protein adsorbed on a given volume.

A final comment on the adsorption results of cyt c on the carbon xerogels shown in Figure 5 is devoted to the differences observed in the protein uptakes measured at 24 h and 96 h. Excluding CX-5 from this discussion, CX-15 and CX-30 show higher protein loadings at 96 h, whereas CX-55 values at 24 h and 96 h are very similar at the three pH buffers, thus suggesting a more favourable kinetics of cyt c adsorption on this meso-macroporous carbon. Results of a more detailed study carried out at pH 10 are shown in Figure 6. Adsorption of cyt c on the three supports was relatively fast during the first hours and slowed down to attain the equilibrium (or, at least, to observe minimum variations in the quantity of protein adsorbed) [43]. The time required to attain the adsorption equilibrium is considerably shorter for CX-55 than for the other two CXs. A closer inspection of the early stages of adsorption is shown in Figure S6. During the first hour of adsorption, the rate of protein loading on both CX-55 and CX-30 is very similar, and significantly faster than the cyt c adsorption on CX-15.

Assuming that the adsorption of the cyt c on the CXs was diffusion controlled, two relatively simple models were used to fit the experimental results of Figure 6, namely the homogeneous diffusion model [43,44]:

$$\ln(1-F) = \ln(6\pi^{-2}) - \pi^2 D_p t R^{-2} \qquad (2)$$

and the parabolic diffusion model [44]:

$$Ft^{-1} = 4D_p^{1/2}\pi^{-1/2}R^{-1}t^{-1/2} - D_p R^{-2} \qquad (3)$$

where F is the fractional loading of cyt C on the CX at time t, D_p is the diffusion coefficient of cyt c on the adsorbent and R is the particle radius (0.05 cm for the CXs, assuming spherical particles). The homogeneous diffusion model (eq. 2) was found to fit reasonably well the experimental points of Figure 6 obtained at $t \geq 60$ min, whereas the parabolic diffusion model (eq. 3) fitted well almost the whole set of points (Figure S7). Results of the D_p values obtained using both models are collected in Table 5. All coefficients are much lower than that of unsupported cyt c in aqueous solution ($2\ 10^{-6}$ $cm^2\ s^{-1}$ at 30 ºC and 100 mM ionic strength) [45]. The information of the two models is quite different. The homogeneous model establishes no significant differences between the diffusion coefficients of the cyt c on the three supports. This situation corresponds to the last stages of adsorption in which diffusion of cyt c is most likely hindered by previously adsorbed biomolecules. On the other hand, the estimation of the D_p based on the parabolic diffusion model reveals a clear difference between the supports, which in turn correlates with the pore size distributions of the CXs. These D_p values would be then closely linked to the pore diffusion of the cyt c on the supports.

3.3. Activity of the supported cyt c

Cyt c is known to catalyse the oxidation of different substrates by H_2O_2 [32-34]. Figure S8 shows the activity profiles of the cyt c used in this work when dissolved in pH 3, pH 6 and pH 10 buffers. Maximum activity values were obtained for the substrates solution buffered at pH 4 [33]. Solutions of cyt c with different pH were tested since it is known that enzymes preserve “memory” of the last aqueous solution they had been dissolved in [46]. As a consequence, in spite of the pH of the solution of the substrates, different enzymatic activities are expected from solutions of the same enzyme prepared at different buffers. This can be seen in Figure S8; the effect of the pH of the cyt c solution is clear, with pH 10 cyt c solutions showing a significantly better performance (using a pH 4 reactants solution) than unsupported cyt c at pH 6 and pH 3.

Immobilised catalysts reproduced such trend (Figure 7), i.e., maximum activities (at pH 4) were obtained when the adsorption of the cyt c on the CXs was carried out at pH 10. It should be noticed that the activities of cyt c/CX-5 were also tested in spite of the very low protein uptakes on this particular material (Figure 5). This leads us to point out a startling result. For a given immobilisation pH, the activity (per gram of support) of all the cyt c/CXs systems is very similar (Figure 7) regardless the huge differences in their protein loadings (Figure 5). In other words, most of the immobilised cyt c on CX-15, -30 and -55 is not operational. In order to clarify this, increasing amounts of cyt c were loaded on the CX-15 and CX-30 supports and the activities of the resulting materials were tested. Activity results (Figure 8) are expressed both in U (g of support)$^{-1}$ and U (mg cyt c)$^{-1}$. The activity results expressed per gram of support were similar for both supports regardless the amount of cyt c adsorbed on them. However, when Units per mg of cyt c are used, the activities improved significantly at low loading values, especially for the CX-15 materials. These activity values are still very far from those of unsupported cyt c solutions, ca. 1 U (mg of cyt c)$^{-1}$. Actually, only CX-5 biocatalysts have similar activities per milligram of cyt c than that of unsupported cyt c (Figure S9 and Figure S8). It should be mentioned here that blank tests were also carried out with

unloaded (pristine) CXs and no activity was detected. These observations would indicate that either there is a limited accessibility of the substrates to the immobilised proteins or that inactivation of cyt c occurs after immobilisation. A series of tests were then devised to understand the lack of activity of most of the cyt c on the CX-15, 30 and 55.

Two cycles of reuse were carried out with the biocatalysts prepared by immobilisation of cyt c solutions buffered at pH 10 (see Section 2.3). Results are also shown in Figure 7. The activity values followed a clear trend, hence increasing substantially after every consecutive cycle for CX-15, CX-30 and CX-55, but decreasing in the case of the CX-5 support. This suggests that successive washings of the heavily loaded supports would "clean" the access to the cyt c stored in the pores. However, it should be mentioned here that such "cleaning" effect would entail a partial lixiviation of the supported enzyme. The amounts of cyt c in the lixiviates were close to the detection limits of the spectrophotometry method used in this work, amounting less than 0.001 mg cyt c mL^{-1} in every wash for all the materials tested. In other words, the amount of cyt c lixiviated from the supports was less than 1 mg of cyt c per gram of support. This number is only relevant for the CX-5 biocatalysts, whose loadings are below 10 mg of cyt c g^{-1} (Figure 5)

A final experiment was carried out with all supports loaded at pH 10 in which the amount of ABTS was increased by an order of magnitude (10 mM) in order to ease the diffusion of the (relative) big reactant inside the porous network. The activity values obtained (Figure 9) show a trend that mimics that already described when successive cycles of reuse were carried out (Figure 7, pH 10). Thus, the CX-15, -30 and -55 systems were more active at higher concentrations of ABTS, whereas the activity of the CX-5 clearly decreased. On the other hand, the activity of unsupported cyt c diminished as the ABTS concentration in the solution increased (see inset in Figure 9).

The outcomes of these two experiments, i.e., the increase of the activity of the CX-15, -30 and -55 in successive re-use cycles (Figure 7) and when, in the first use, the concentration of ABTS is 10 mM (Figure 9), led us to propose the following model of cyt c adsorption. Minimum quantities (ca. 5 mg g^{-1}, Figure 5) of cyt c are adsorbed on the external (geometrical) surface of CX-5 particles. These biomolecules behave essentially as unsupported cyt c, hence the similar dependence on ABTS concentration and the reduction of the supported cyt c activity with reuse due to progressive leaching, which although being very low is more significant for the CX-5 systems. For the rest of supports, the explanation is a bit more complex. Thus, the improvement of the activity of the immobilised cyt c when working at high concentrations of ABTS (Figure 9) would support, in principle, the hypothesis of the limited accessibility of the reactants to the cyt c hosted within the pores. Certainly, an increase of ABTS concentration in the solution should favour the diffusion of the ABTS molecules inside the pores. This simple explanation, however, does not fit with the behaviour observed for the unsupported cyt c solutions (inset of Figure 9). If the activity of the cyt c located in the pores of the CX-15, -30 and -55 were similar to that of unsupported cyt c, the activity values of the resulting materials should not increase when the concentration of ABTS increases. Moreover, if partial pore clogging is responsible for the low activity (per mg of cyt c) of the supports with pores ≥ 15 nm, this effect should be affected by the relative pore filling percentages (Table 4), with CX-55 biocatalysts having much less restrictions than CX-15 ones, which is not the case.

A model that would explain the activity results observed for the cyt c supported on CX-15, -30 and -55 should include both a gradient in the concentration and in the *activity* of the adsorbed cyt c molecules. Hence, in all these systems a given amount of cyt c would be adsorbed on their geometrical (external) surfaces, in a similar fashion (and possibly quantity) than in CX-5. Under the initial selected conditions of operation, at

relatively low (1 mM) ABTS concentration, the activity of the materials would also be determined by that external layer of adsorbed cyt c. When the ABTS concentration increases (10 mM, Figure 9) diffusion of the substrate is favoured, and trapped cyt c would oxidise ABTS faster. This suggests a high stabilisation of the biomolecules inside the pores that would show a higher activity than cyt c in solution [47]. Alternatively, when successive reuses of the CX-15, CX-30 and CX-55 help to remove the cyt c adsorbed on the outer layers of the carbons (as in the case of CX-5), ABTS (1 mM) would have access to cyt c biomolecules having higher activity as a consequence of their confinement inside the pore network, hence the increase observed (Figure 7, pH 10).

4. Conclusions

The synthesis of carbon xerogels with narrow PSDs and the control of their average pore size over the whole mesopores range provide an ideal set of materials for studying the interaction of carbon surfaces with proteins. Several novel outcomes derived from this study. Pore sizes well over the size of the protein are more indicated for hosting biomolecules, both in terms of quantity adsorbed and favourable kinetics. Accordingly, the CX-5 materials (with 5 nm average pore size) adsorbed very little amounts of cyt c (below 10 mg g^{-1}), which was expected to lay on the external surface of the carbon particles. This result is at odds with several studies carried out on nanostructured mesoporous carbons with similar average pore sizes.

The interaction of the basic, highly pure carbon surfaces of the CXs with the proteins was essentially hydrophobic, i.e., it was independent of the pH of the solution used for the immobilisation. This also contradicts previous studies that claimed maximum adsorption capacities when using cyt c solutions buffered at pHs close to the isoelectric

point of the protein (10.5 for cyt c). On the contrary, the ionic strength of the cyt c solution influenced considerably the adsorption of the protein on the CXs.

Finally, high protein loadings on the CXs did not entail high catalytic activities of the resulting materials. The activity of cyt c supported on all CXs was essentially the same regardless the pore size and/or pore volume (hence the protein uptakes) of the four supports. Additional studies, however, demonstrated a very different behaviour of the cyt c supported on CX-5, on one side, and on the rest of systems (CX-15, -30 and -55) on the other. Thus, cyt c adsorbed on CX-5 behaved like unsupported cyt c. In the case of the cyt c adsorbed on the rest of CXs, the situation is more complex. Under conventional test conditions, the catalytic activity of all the systems studied was highly controlled by the biomolecules adsorbed on the external surface of the materials. However, when higher concentrations of the substrate (ABTS) were used or when successive cycles of reuse were carried out, a rise on the activity of the cyt c/CX-15, -30 and -55 systems was observed. The combination of results from these last experiments suggested that not only the access of ABTS to the cyt c adsorbed on the pores was favoured, but that the activity of those “trapped” cyt c molecules was higher than that of the protein adsorbed on the external surface of the support and, hence, of the unsupported protein.

Acknowledgments

This work was funded by the PCTI-Asturias (Project GRUPIN14-117). LARM thanks CONACYT (México) for a post-doctoral grant (CVU No 330625, 2016).

Supporting Information Available

Nine figures are included.

References

[1] Klibanov AM. Enzyme stabilization by immobilization. Anal Biochem 1979;93:1-25.

[2] Tran DN, Balkus Jr KJ. Perspective of recent progress in immobilization of enzymes. ACS Catal 2011;1:956-968.

[3] Kyotani T. Control of pore structure in carbon. Carbon 2000;38:269-286.

[4] Cho YK, Bailey JE. Immobilization of enzymes on activated carbon: selection and preparation of the carbon support. Biotechnol Bioeng 1979;21:461-476.

[5] Nagy B, Tóth A, Savina I, Mikhalovsky S, Mikhalovska L, Geissler E, László K. Double probe approach to protein adsorption on porous carbon surfaces. Carbon 2017;112:103-110.

[6] Nagy B, Tóth A, Savina I, Mikhalovsky S, Mikhalovska L, Grillo I, Geissler E, László K. Small angle neutron scattering study of globular proteins confined in porous carbons. Carbon 2016;106:142-151.

[7] Enterría M, Figueiredo JL. Nanostructured mesoporous carbons: tuning texture and surface chemistry. Carbon 2016;108:79-102.

[8] Liang C. Li Z, Dai S. Mesoporous carbon materials: synthesis and modification. Angew Chem Int Ed 2008;47:3696-3717.

[9] Lee J, Kim J, Hyeon T. Recent progress in the synthesis of porous carbon materials. Adv Mater 2006;18:2073-2094.

[10] Vinu A, Streb C, Murugesan V, Hartmann M. Adsorption of cytochrome c on new mesoporous carbon molecular sieves. J Phys Chem B 2003;107:8297-8299.

[11] Vinu A, Miyahara M, Ariga K. Biomaterial immobilization in nanoporous carbon molecular sieves: influence of solution pH, pore volume, and pore diameter. J Phys Chem B 2005;109:6436-6441.

[12] Vinu A, Hossain KZ, Kumar GS, Ariga K. Adsorption of L-histidine over mesoporous carbon molecular sieves. Carbon 2006;44:530-536.

[13] Vinu A, Hossain KZ, Srinivasu P, Miyahara M, Anandan S, Gokulakrishnan N, Mori T, Ariga K, Balasubramanian VV. Carboxy-mesoporous carbon and its excellent adsorption capability for proteins. J Mater Chem 2007;17:1819-1825.

[14] Díaz JF, Balkus Jr KJ. Enzyme immobilization in MCM-41 molecular sieve. J Mol Catal B:Enzymatic 1996;2:115-126.

[15] Deere J, Magner E, Wall JG, Hodnett BK. Adsorption and activity of cytochrome c on mesoporous silicates. Chem Comm 2001:465-466.

[16] Washmon-Kriel L, Jimenez VL, Balkus Jr KJ. Cytochrome c immobilization into mesoporous molecular sieves. J Mol Cat B:Enzymatic 2000;10:453-469.

[17] Blanco RM, Terreros P, Fernández-Pérez M, Otero C, Díaz-González G. Functionalization of mesoporous silica for lipase immobilization Characterization of the support and the catalysts. J Mol Cat B:Enzymatic 2004;30:83-93.
[18] Hudson S, Magner E, Cooney J, Hodnett BK. Methodology for the immobilization on enzymes onto mesoporous materials. J Phys Chem B 2005;109:19496-19506.
[19] Hudson S, Cooney J, Magner E. Proteins in mesoporous silicates. Angew Chem Int Ed 2008;47:8582-8594.
[20] Rodríguez-Reinoso F. The role of carbon materials in heterogeneous catalysis. Carbon 1998;36:159-175.
[21] Quirós M, García AB, Montes-Morán MA. Influence of the support surface properties on the protein loading and activity of lipase/mesoporous carbon biocatalysts. Carbon 2011;49:406-415.
[22] Bayne L, Ulijn RV, Halling PJ. Effect of pore size on the performance of immobilised enzymes. Chem Soc Rev 2013;42:9000-9010.
[23] Zhao J, Wang Y, Luo G, Zhu S. Immobilization of penicillin G acylase on macro-mesoporous silica spheres. Bioresource Technology 2011;102:529-535.
[24] Lazzara TD, Mey I, Steinem C, Janshoff A. Benefits and limitations of porous substrates as biosensors for protein adsorption. Anal Chem 2011;83:5624-5630.
[25] Rey-Raap N, Menéndez JA, Arenillas A. Simultaneous adjustment of the main chemical variables to fine-tune the porosity of carbon xerogels. Carbon 2014;78:490-499.
[26] Rey-Raap N, Menéndez JA, Arenillas A. RF xerogels with tailored porosity over the entire nanoscale. Mic Mes Mater 2014;195:266-275.
[27] Calvo EG, Juárez-Pérez EJ, Menéndez JA, Arenillas A. Fast microwave-assisted synthesis of tailored mesoporous carbon xerogels. J Coll Interf Sci 2011;357:541-547.
[28] Menéndez JA, Illán-Gómez MJ, León y León CA, Radovic LR. On the difference between the isoelectric point and the point of zero charge of carbons. Carbon 1995;33:1655-1659.
[29] Estrade-Szwarckopf H. XPS photoemission in carbonaceous materials: a “defect” peak beside the graphitic asymmetric peak. Carbon 2004;42:1713-1721.
[30] Figueiredo JL, Pereira MFR, Freitas MMA, Órfão JJM. Characterization of active sites on carbon catalysts. Ind Eng Chem Res 2007;46:4110-4115.
[31] Bonde M, Pontoppidan H, Pepper DS. Direct dye binding-A quantitative assay for solid-phase immobilized protein. Anal Biochem 1992;200:195-198.
[32] Tu AT, Reinosa JA, Hsiao YY. Peroxidative activity of hemepeptides from horse heart cytochrome c. Experientia 1968;24:219-221.

[33] Radi R, Thomson L, Rubbo H, Prodanov E. Cytochrome c-catalyzed oxidation of organic molecules by hydrogen peroxide. Arch Biochem Biophys 1991;288:112-117.
[34] Vazquez-Duhalt R. Cytochrome c as biocatalyst. J Mol Cat B:Enzymatic 1999;7:241-249.
[35] Rey-Raap N, Arenillas A, Menéndez JA. A visual validation of the combined effect of pH and dilution on the porosity of carbon xerogels. Mic Mes Mater 2016;223:89-93.
[36] Moreno-Castilla C, Carrasco-Marín F, Mueden A. The creation of acid carbon surfaces by treatment with $(NH_4)_2S_2O_8$. Carbon 1997;35:1619-1626.
[37] Fan J, Lei J, Wang L, Yu C, Tu B, Zhao D. Rapid and high-capacity immobilization of enzymes based on mesoporous silicas with controlled morphologies. Chem Comm 2003:2140-2141.
[38] Vijayaraj M, Gadiou R, Anselme K, Ghimbeu C, Vix-Gurtel C, Orikasa H, Kyotani T, Ittisanronnachai S. The influence of surface chemistry and pore size on the adsorption of proteins on nanostructured carbon materials. Adv Func Mater 2010;30:2489-2499.
[39] Bushnell GW, Louie GV, Brayer GD. High-resolution three-dimensional structure of horse heart cytochrome c. J Mol Biol 1990;214:585-595.
[40] Sang L-C, Vinu A, Coppens M-O. General description of the adsorption of proteins at their iso-electric point in nanoporous materials. Langmuir 2011;27:13828-13837.
[41] Montes-Morán MA, Suárez D, Menéndez JA, Fuente E. The basicity of carbons. In: Tascón JMD, editor. Novel Carbon Adsorbents. Oxford: Elsevier; 2012. p. 173-203.
[42] Eriksson K-O, Belew M. Hydrophobic interaction chromatography. In: Janson J-C, editor. Protein purification. New Jersey: John Wiley&Sons; 2011(3rd edition). p. 165-181.
[43] Ivanov AE, Kozynchenko OP, Mikhalovska LI, Tennison SR, Jungvid H, Gun'ko VM, Mikhalovsky SV. Activated carbons and carbon-containing poly(vinyl alcohol) cryogels: characterization, protein adsorption and possibility of myoglobin clearance. Phys Chem Chem Phys 2012;14:16267-16278.
[44] Trgo M, Perić J, Medvidović NV. A comparative study of ion exchange kinetics in zinc/lead-modified zeolite-clinoptilolite systems. J Haz Mat 2006;B136:938-945.
[45] Kontturi A-K, Kontturi K, Niinikoski P, Savonen A, Vuoristo M. The effective charge number and diffusion coefficient of cationic cytochrome c in aqueous solution. Acta Chem Scandinavica 1992;46:348-353.
[46] Zaks A, Klibanov AM. Enzyme-catalyzed processes in organic solvents. Proc Natl Acad Sci USA 1985;82:3192-3196.

[47] Sang L-C, Coppens M-O. Effects of surface curvature and surface chemistry on the structure and activity of proteins adsorbed in nanopores. Phys Chem Chem Phys 2011;13:6689-6698.

Table 1. Experimental variables used in the preparation of the organic xerogels (OXs) that were carbonised to obtain the different carbon xerogels (CXs).

Sample	R/F ratio	D[a]	pH	MeOH (%)[b]
CX-5	0.5	5.7	6.5	20
CX-15	0.1	6.7	6.25	10
CX-30	0.15	6.7	5.4	10
CX-55	0.3	8	6	12.5

[a] Dilution ratio (see text)
[b] Methanol content of the formaldehyde solution

Table 2. Textural parameters of the carbon xerogels.

Sample	S_{BET} ($m^2\ g^{-1}$)	V_{total}[a] ($cm^3\ g^{-1}$)	V_{DR}[b] ($cm^3\ g^{-1}$)	V_{meso}[c] ($cm^3\ g^{-1}$)	ρ_{He} ($g\ cm^{-3}$)	V_{Hg}[d] ($cm^3\ g^{-1}$)	ρ_{Hg} ($g\ cm^{-3}$)	s[e] (%)
CX-5	660	0.71	0.23	0.48	1.69	-	1.05	38
CX-15	679	1.16	0.26	0.90	1.75	0.88	0.61	65
CX-30	625	1.42	0.24	1.18	1.78	1.32	0.46	74
CX-55	640	0.78	0.24	0.54	1.74	1.48	0.43	75

[a] Calculated at $p/p_0 = 0.99$
[b] DR: Dubinin-Radushkevich model
[c] $V_{meso} = V_{total} - V_{DR}$
[d] Hg intrusion pore volume corresponding to the pore size distributions shown in Figure 2
[e] Open porosity (eq. 1)

Table 3. XPS and TPD results on the composition of the carbon xerogels

Sample	XPS Atom%		TPD CO ($\mu mol\ g^{-1}$)	TPD CO_2 ($\mu mol\ g^{-1}$)
	C	O		
CX-5	94.2	5.8	243	159
CX-15	96.0	4.0	255	247
CX-30	95.8	4.2	277	283
CX-55	95.8	4.2	260	217

Table 4. Average values of the protein loadings (volumetric basis) on CXs at 96 h. Pore filling percentages are in parentheses.

Sample	Protein loading ($mg\ cm^{-3}$)		
	pH 3	pH 6	pH 10
CX-5	8 (5%)	12 (7%)	4 (2%)
CX-15	123 (73%)	174 (100%)	144 (85%)
CX-30	137 (80%)	120 (70%)	114 (70%)
CX-55	103 (61%)	71 (42%)	61 (36%)

Table 5. Diffusion coefficients of cyt c adsorption on CXs calculated from the homogeneous and parabolic diffusion models Correlation coefficients of the model fitting are also included.

Sample	Homogeneous Diffusion (eq. 2)[a]		Parabolic Diffusion (eq. 3)	
	$D_p \times 10^9$ cm^2 s^{-1}	R^2	$D_p \times 10^9$ cm^2 s^{-1}	R^2
CX-15	3.8	0.994	1.4	0.995
CX-30	3.1	0.991	7.7	0.996
CX-55	2.5	0.982	25	0.999

[a] For experimental points obtained at t ≥ 60 min (see text)

FIGURE CAPTIONS

FIGURE 1. N_2 adsorption/desorption isotherms at -196 ºC of the CXs.
FIGURE 2. Pore size distributions of the CXs as measured by Hg intrusion porosimetry.
FIGURE 3. High resolution C1s XPS profiles of the four carbon supports.
FIGURE 4. TPD (a) CO and (b) CO_2 profiles of the CXs.
FIGURE 5. Cyt c loadings (average values and errors), expressed as mg of biomolecule per gram of support, on the four CXs after 24 and 96 h of adsorption. Experimental conditions: initial concentration of the solutions, 0.5 g cyt c L^{-1}; temperature, 30 ºC; ionic strength of the different buffers, 100 mM.
FIGURE 6. Kinetics of adsorption of cyt c on CX-15, CX-30 and CX-55. Experimental conditions: initial concentration of the solutions, 0.5 g cyt c L^{-1}; temperature, 30 ºC; pH 10 (100 mM ionic strength).
FIGURE 7. Activities expressed as Units per gram of support. The biocatalysts were prepared by immobilisation of cyt c on CXs at different pH (pH 3, 6 and 10). All the activity tests were carried out at pH 4.
FIGURE 8. Activities of CX-15 and CX-30 materials prepared by immobilisation of different quantities of cyt c on them at pH 10. Circles correspond to activities expressed in Units per g of support (left y axis), whereas triangles correspond to activities expressed in Units per mg of cyt c (right y axis). All the activity tests were carried out at pH 4.
FIGURE 9. Effect of the ABTS concentration on the activity (expressed as Units per g of support) of CXs biocatalysts prepared at pH 10. Inset: effect of the ABTS concentration on the activity of unsupported cyt c (0.5 g L^{-1}, 30 ºC, pH 10, 100 mM). All the activity tests (including unsupported cyt c experiments) were carried out at pH 4.

FIGURE 1

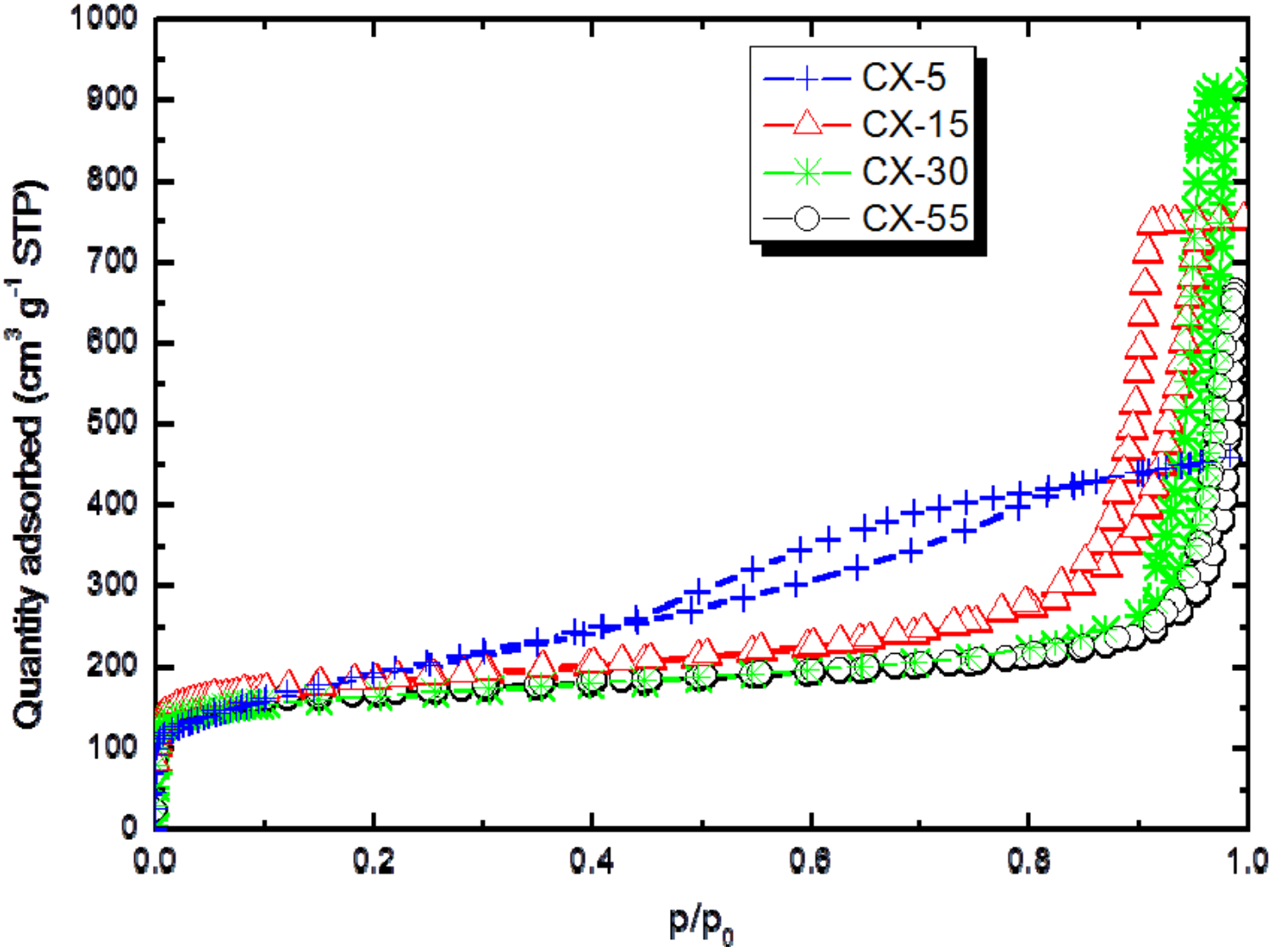
CX-5
CX-15
CX-30
CX-55
Quantity adsorbed (cm^3 g^{-1} STP)
p/p$_0$
0
100
200
300
400
500
600
700
800
900
1000
0.0
0.2
0.4
0.6
0.8
1.0

FIGURE 2

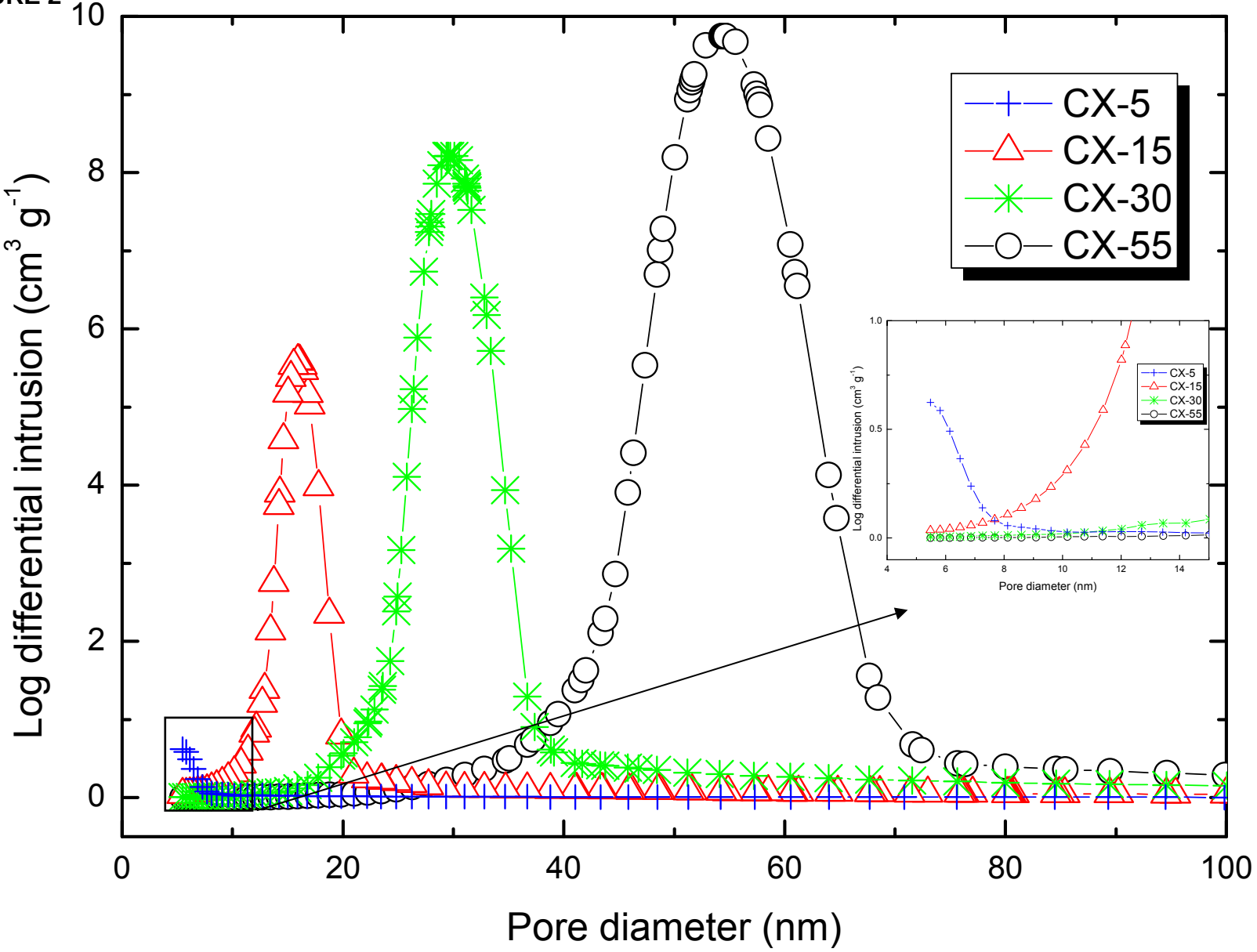
Log differential intrusion (cm3 g-1)
Pore diameter (nm)
CX-5
CX-15
CX-30
CX-55
0
2
4
6
8
10
0
20
40
60
80
100
Log differential intrusion (cm3 g-1)
Pore diameter (nm)
0.0
0.5
1.0
4
6
8
10
12
14

FIGURE 3

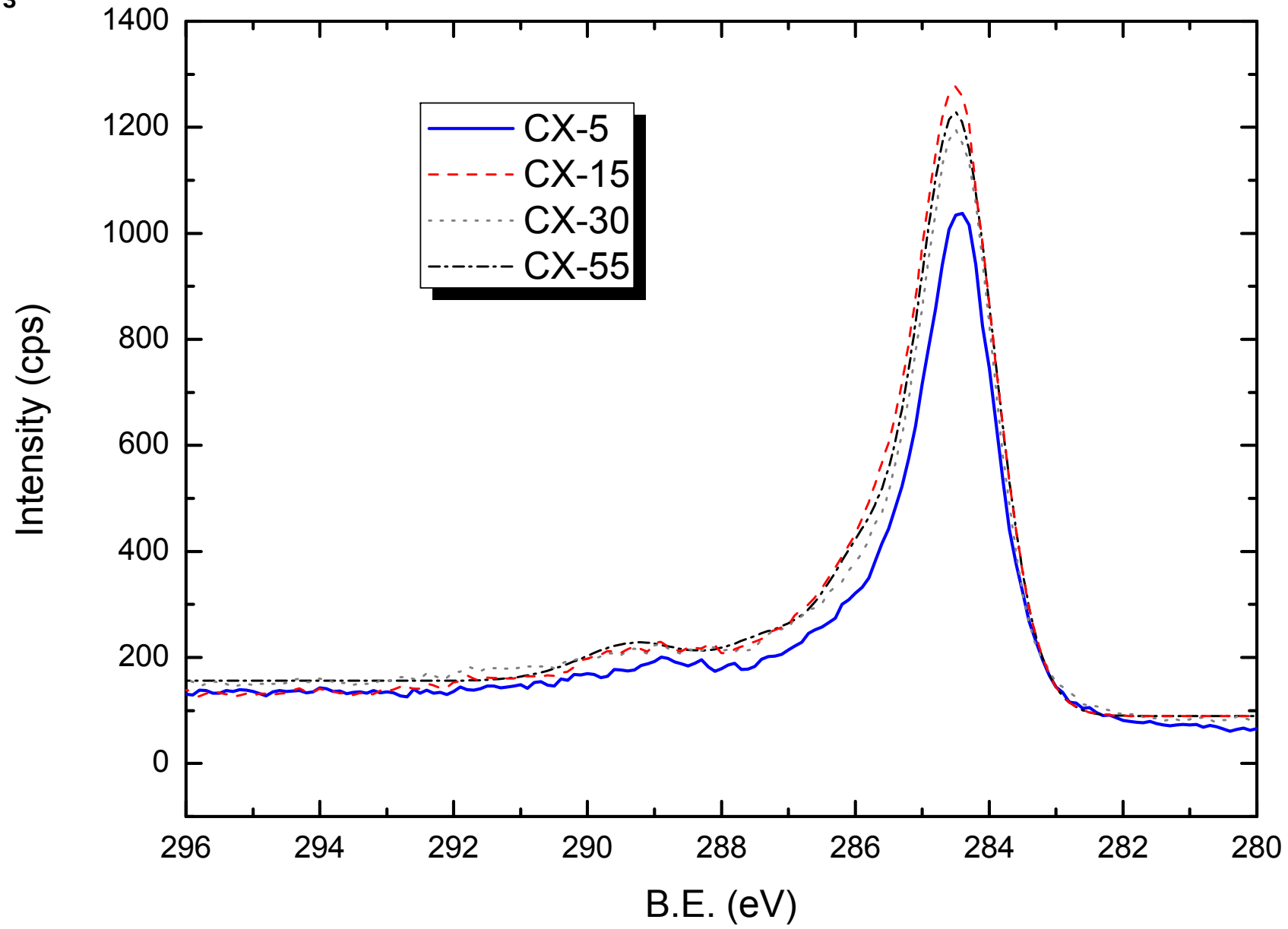
CX-5
CX-15
CX-30
CX-55
Intensity (cps)
B.E. (eV)
1400
1200
1000
800
600
400
200
0
296
294
292
290
288
286
284
282
280

FIGURE 4

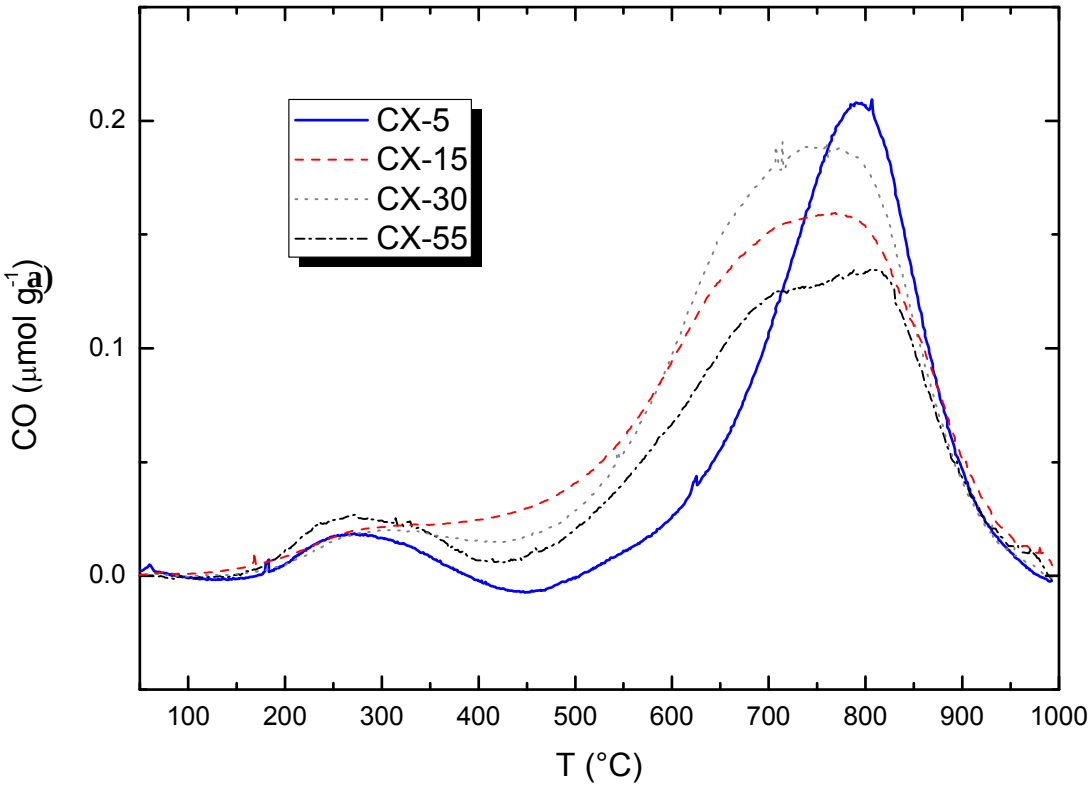
a)
CX-5
CX-15
CX-30
CX-55
CO (μmol g-1)
0.0
0.1
0.2
100
200
300
400
500
600
700
800
900
1000
T (°C)

b)

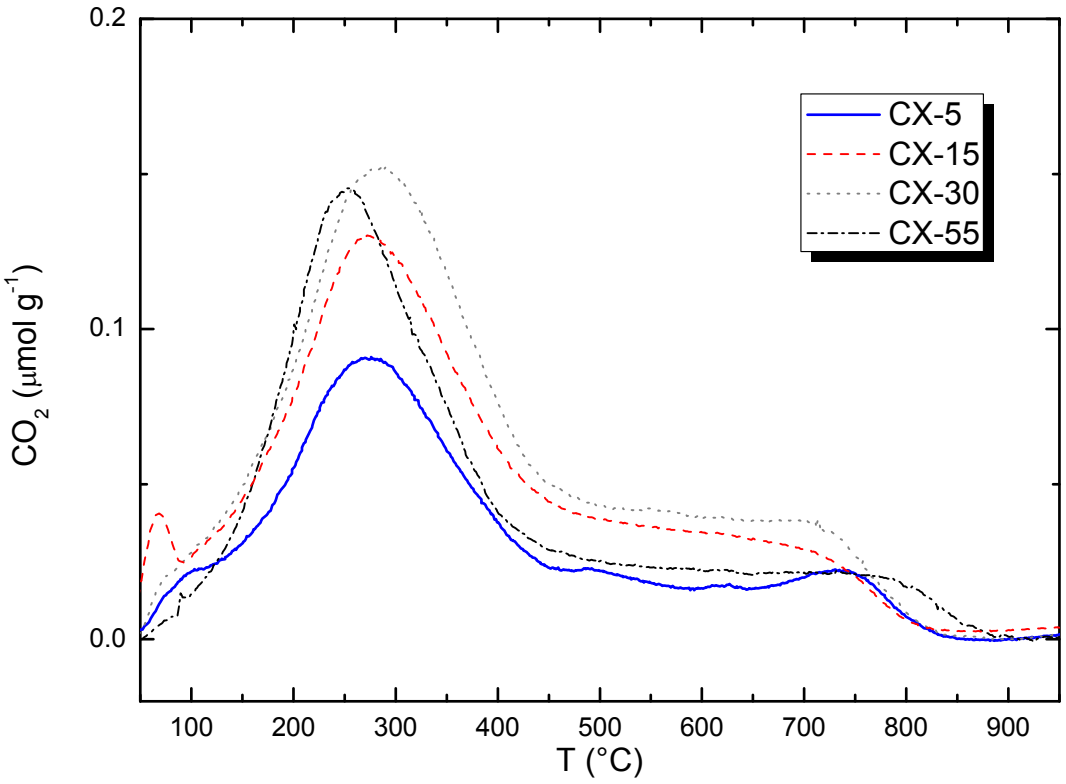
CX-5
CX-15
CX-30
CX-55
CO2 (μmol g-1)
0.0
0.1
0.2
100
200
300
400
500
600
700
800
900
T (°C)

FIGURE 5

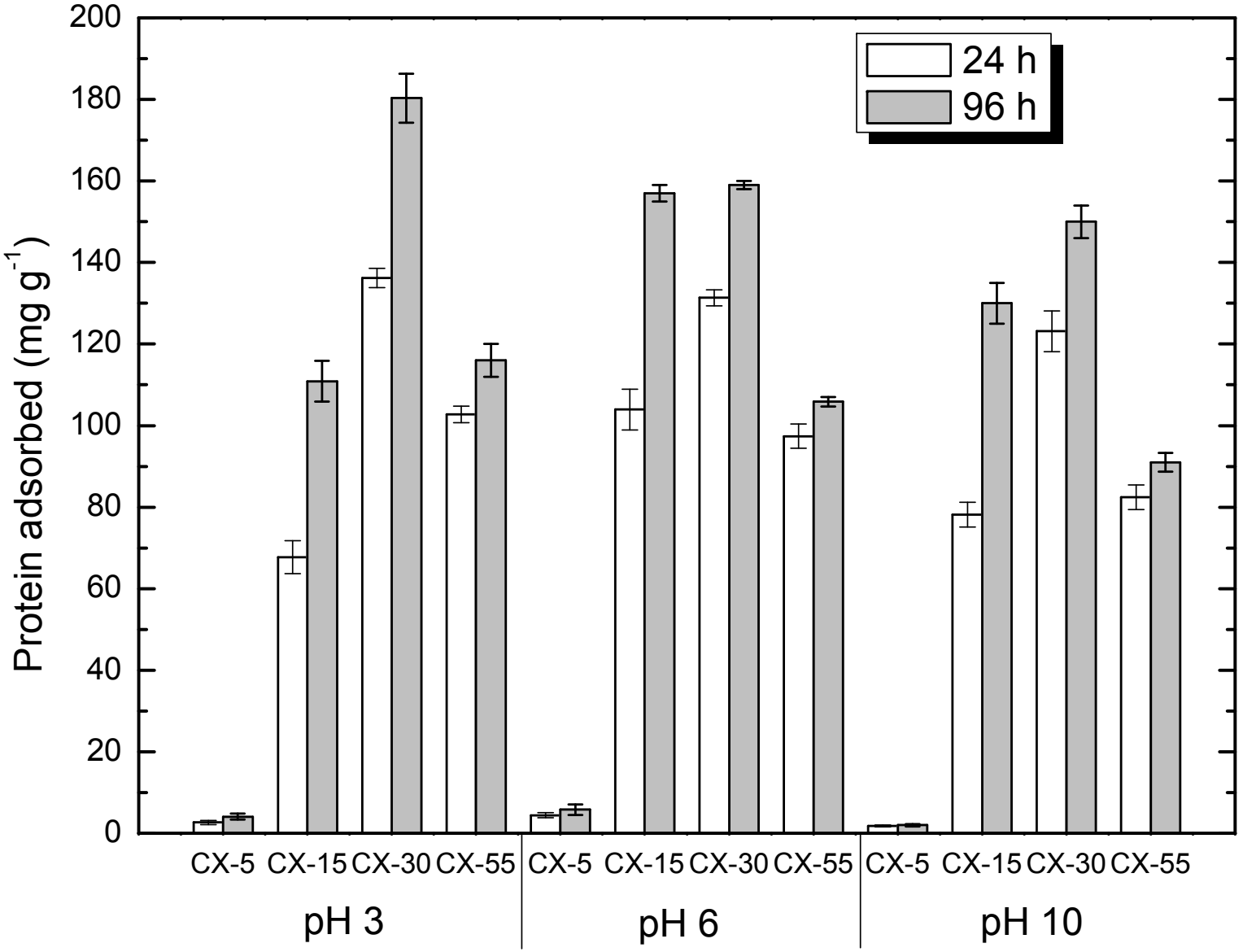
Protein adsorbed (mg g-1)
200
180
160
140
120
100
80
60
40
20
0
24 h
96 h
CX-5
CX-15
CX-30
CX-55
CX-5
CX-15
CX-30
CX-55
CX-5
CX-15
CX-30
CX-55
pH 3
pH 6
pH 10

FIGURE 6

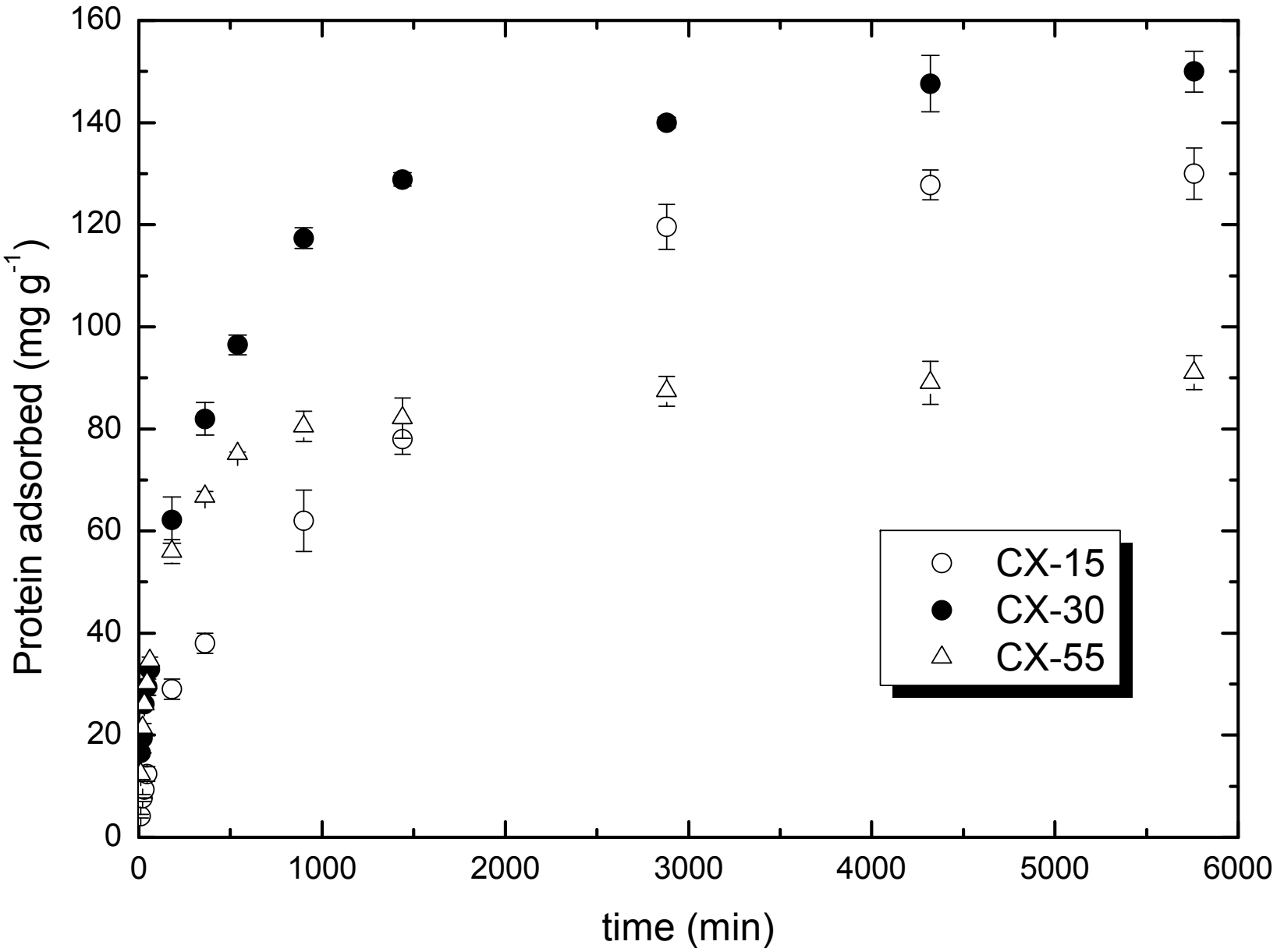
Protein adsorbed (mg g-1)
time (min)
0
20
40
60
80
100
120
140
160
0
1000
2000
3000
4000
5000
6000
CX-15
CX-30
CX-55

FIGURE 7

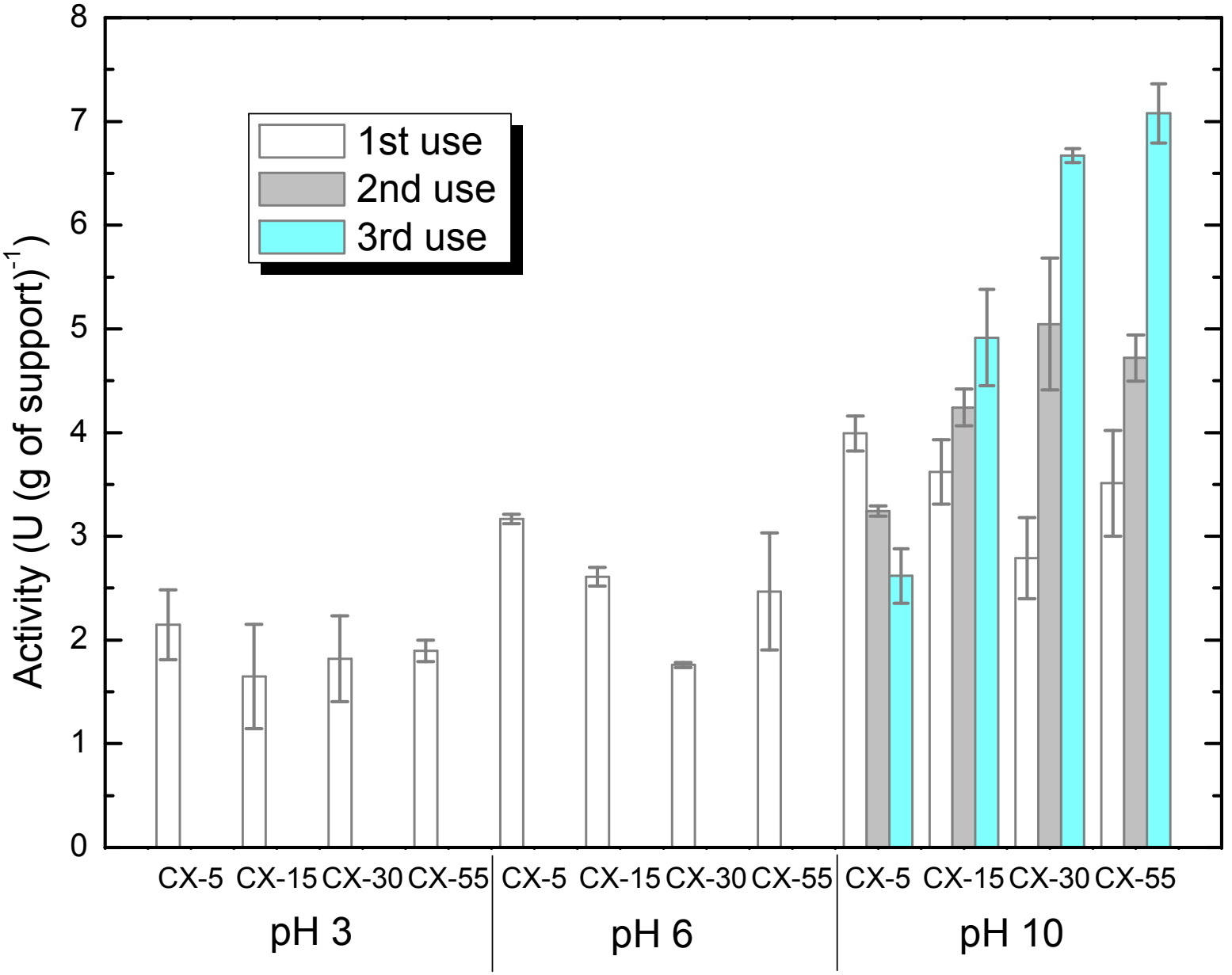
Activity (U (g of support)$^{-1}$)
0
1
2
3
4
5
6
7
8
1st use
2nd use
3rd use
CX-5
CX-15
CX-30
CX-55
CX-5
CX-15
CX-30
CX-55
CX-5
CX-15
CX-30
CX-55
pH 3
pH 6
pH 10

FIGURE 8

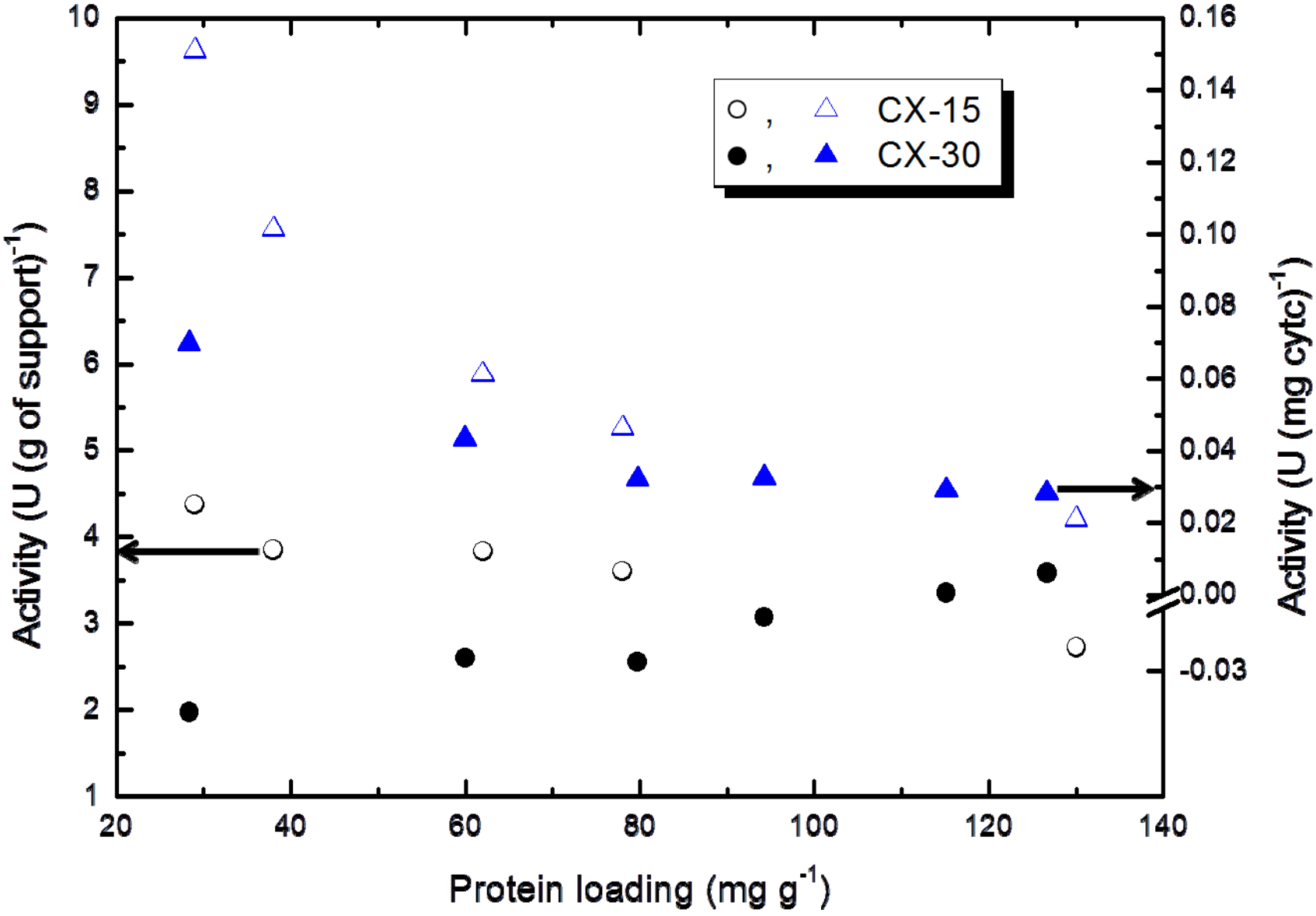
Activity (U (g of support)$^{-1}$)
Activity (U (mg cytc)$^{-1}$)
Protein loading (mg g^{-1})
CX-15
CX-30
10
9
8
7
6
5
4
3
2
1
0.16
0.14
0.12
0.10
0.08
0.06
0.04
0.02
0.00
-0.03
20
40
60
80
100
120
140

FIGURE 9

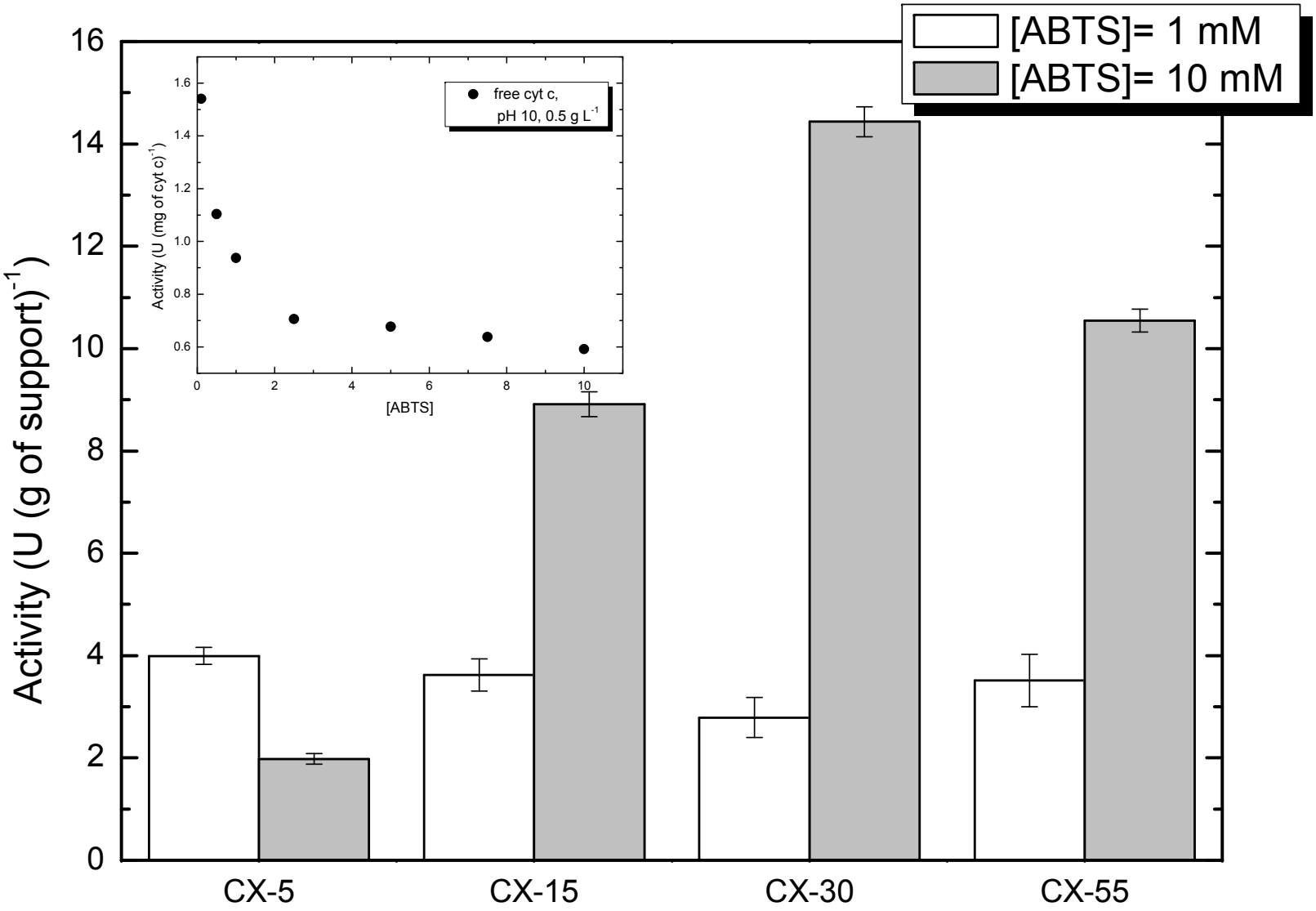
[ABTS]= 1 mM
[ABTS]= 10 mM
Activity (U (g of support)$^{-1}$)
0
2
4
6
8
10
12
14
16
CX-5
CX-15
CX-30
CX-55
free cyt c,
pH 10, 0.5 g L^{-1}
Activity (U (mg of cyt c)$^{-1}$)
0.6
0.8
1.0
1.2
1.4
1.6
0
2
4
6
8
10
[ABTS]

FIGURE S1. Hg intrusion volumes of the CXs.

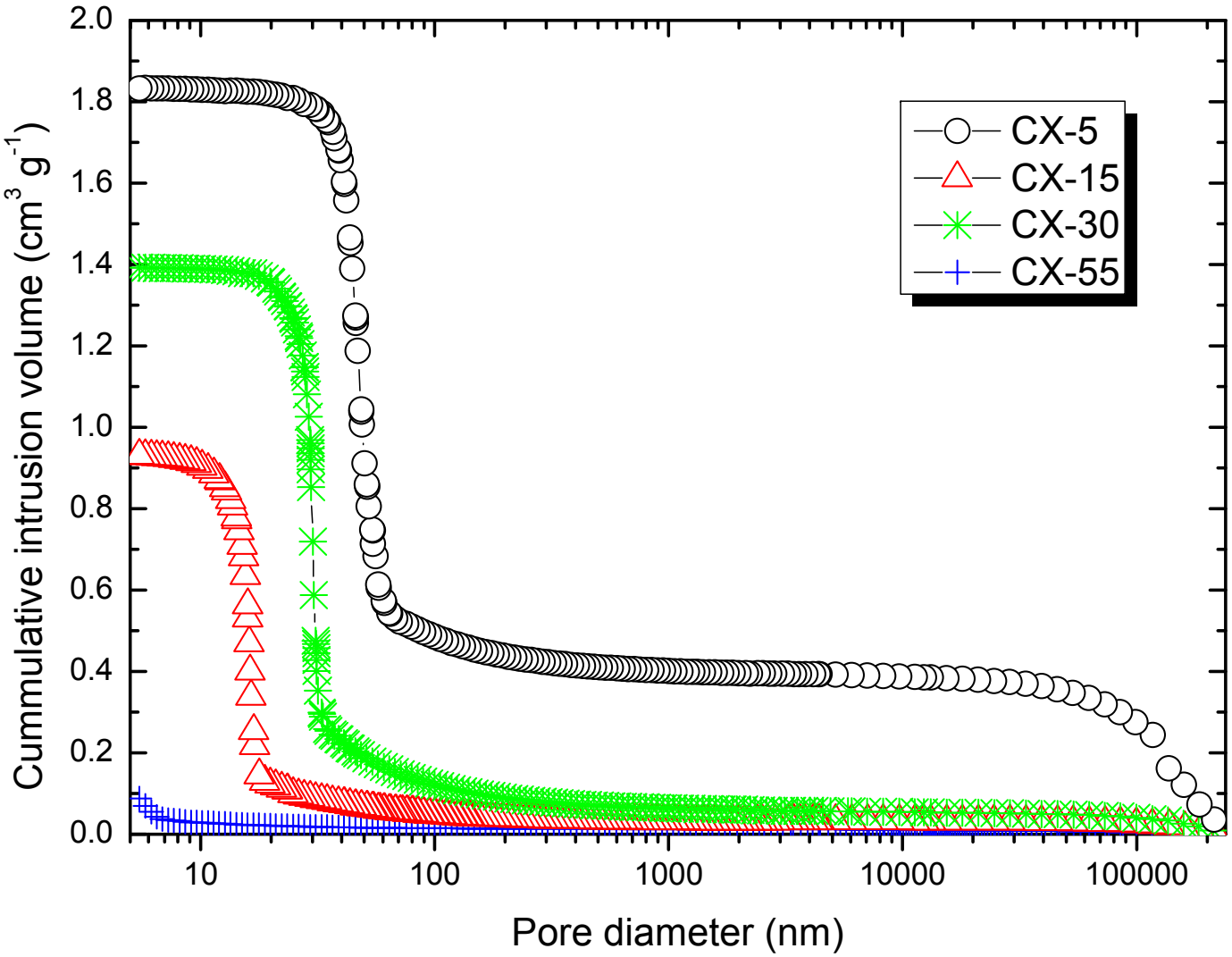

FIGURE S2. Pore size distribution of the CXs as determined by DFT modelling of the N_2 adsorption isotherm.

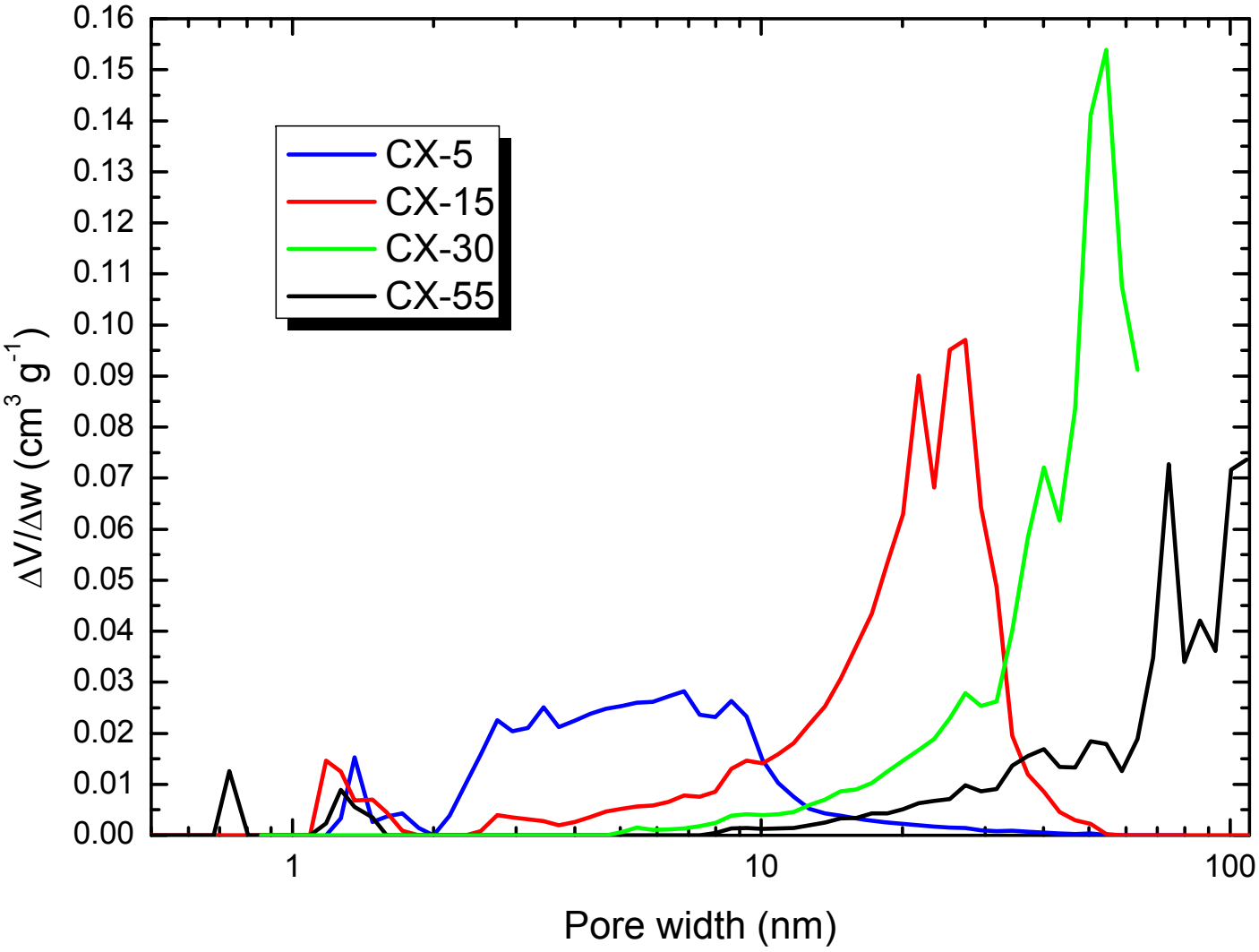

FIGURE S3. Deconvolution of the high resolution C1s XPS profile of CX-5.

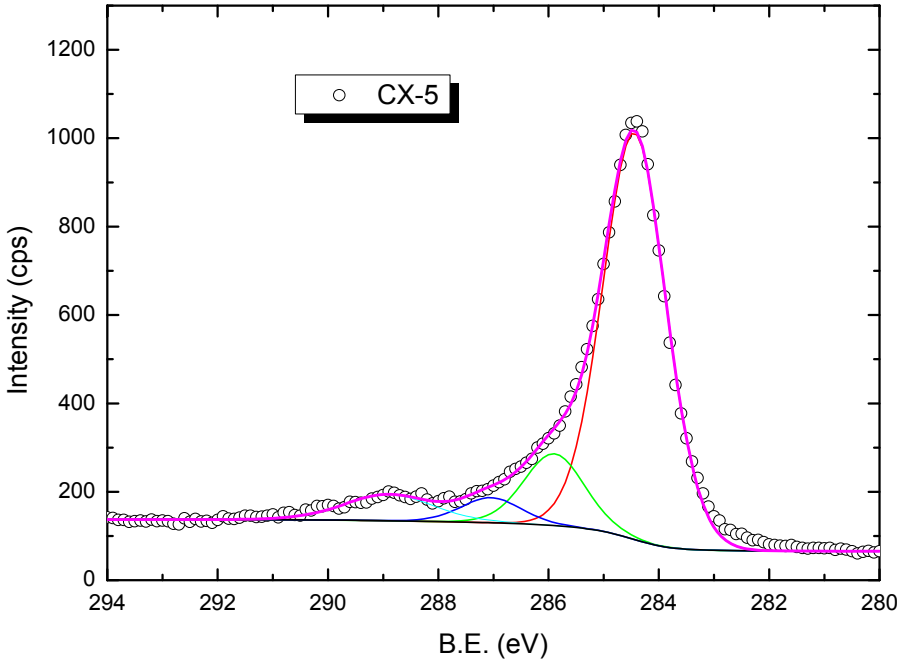

FIGURE S4. Deconvolution of the TPD (a) CO and (b) CO_2 profiles of the CX-55.

a)

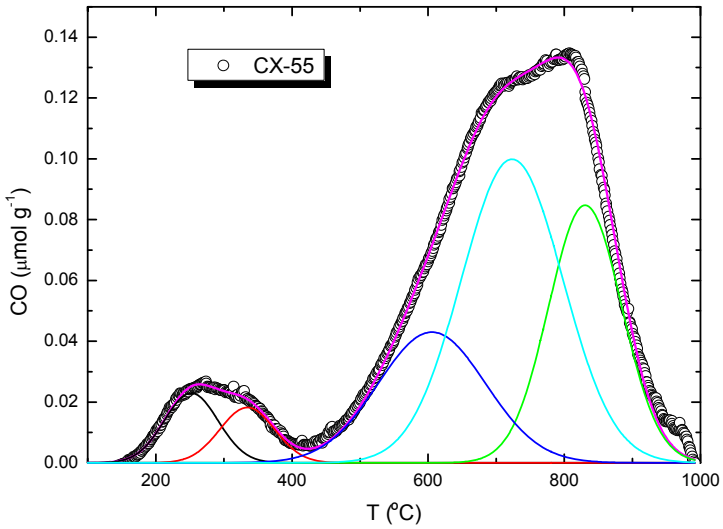

b)

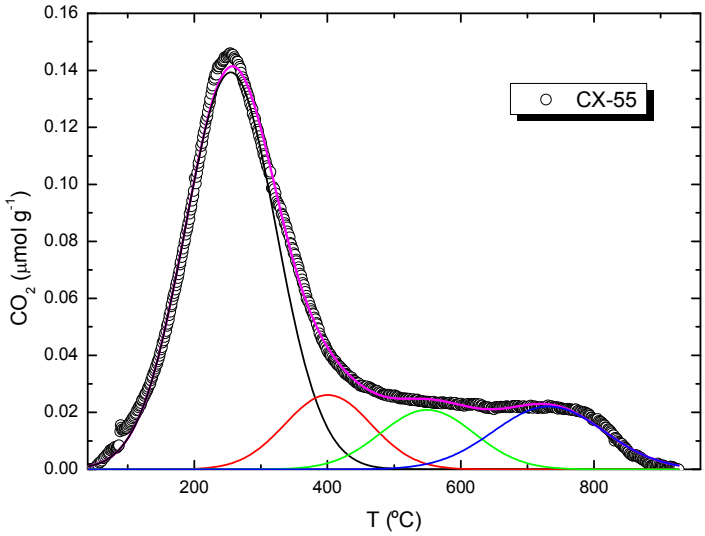

FIGURE S5. Cyt c loadings (average values and errors), expressed as mg of biomolecule per gram of support, on the four CXs after 24 and 96 h of adsorption as determined by the Bio-Rad method. Experimental conditions: initial concentration of the solutions, 0.5 g cyt c L^{-1}; temperature, 30 ºC; ionic strength of the different buffers, 100 mM.

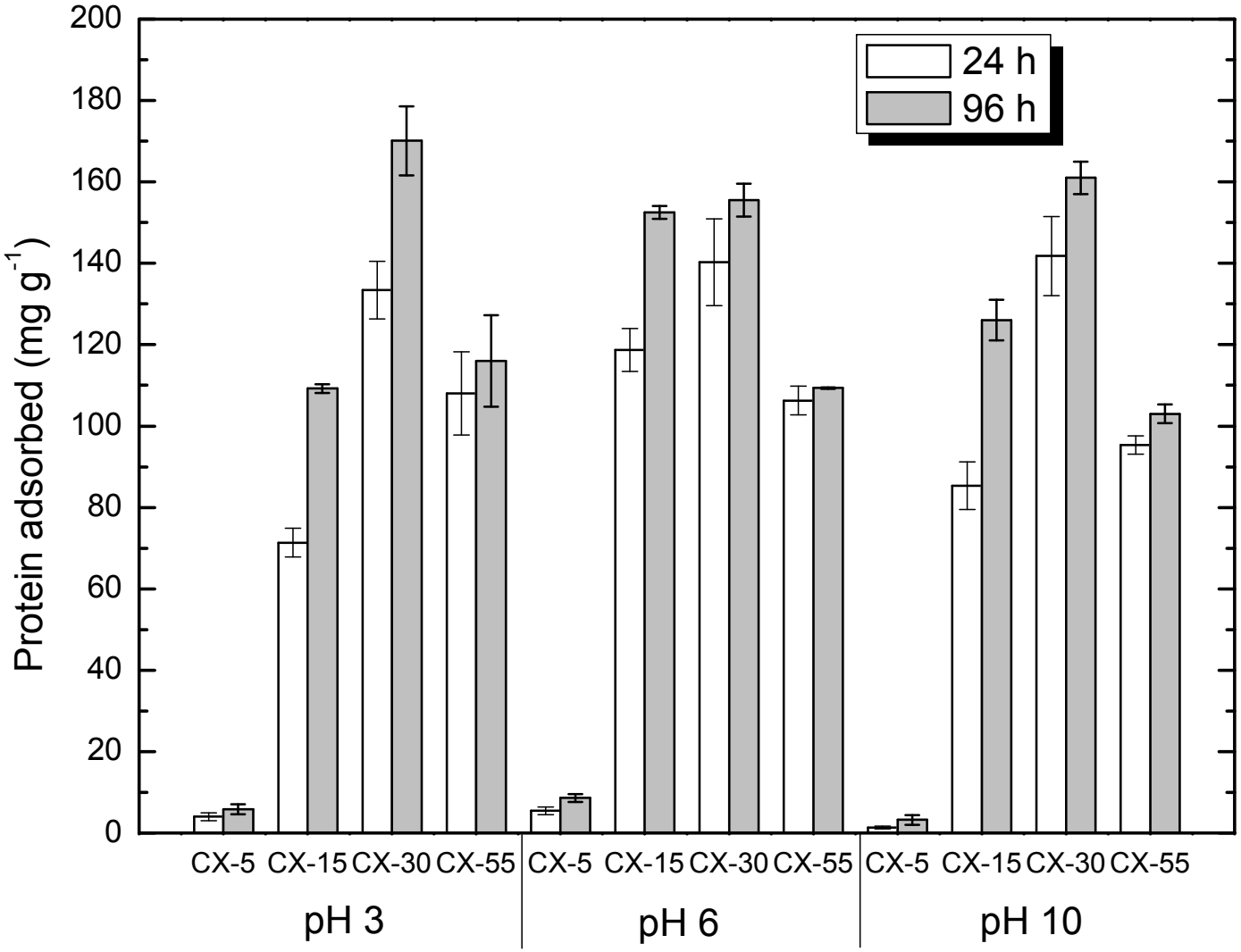

FIGURE S6. Detail of Figure 6 corresponding to the initial stages of adsorption.

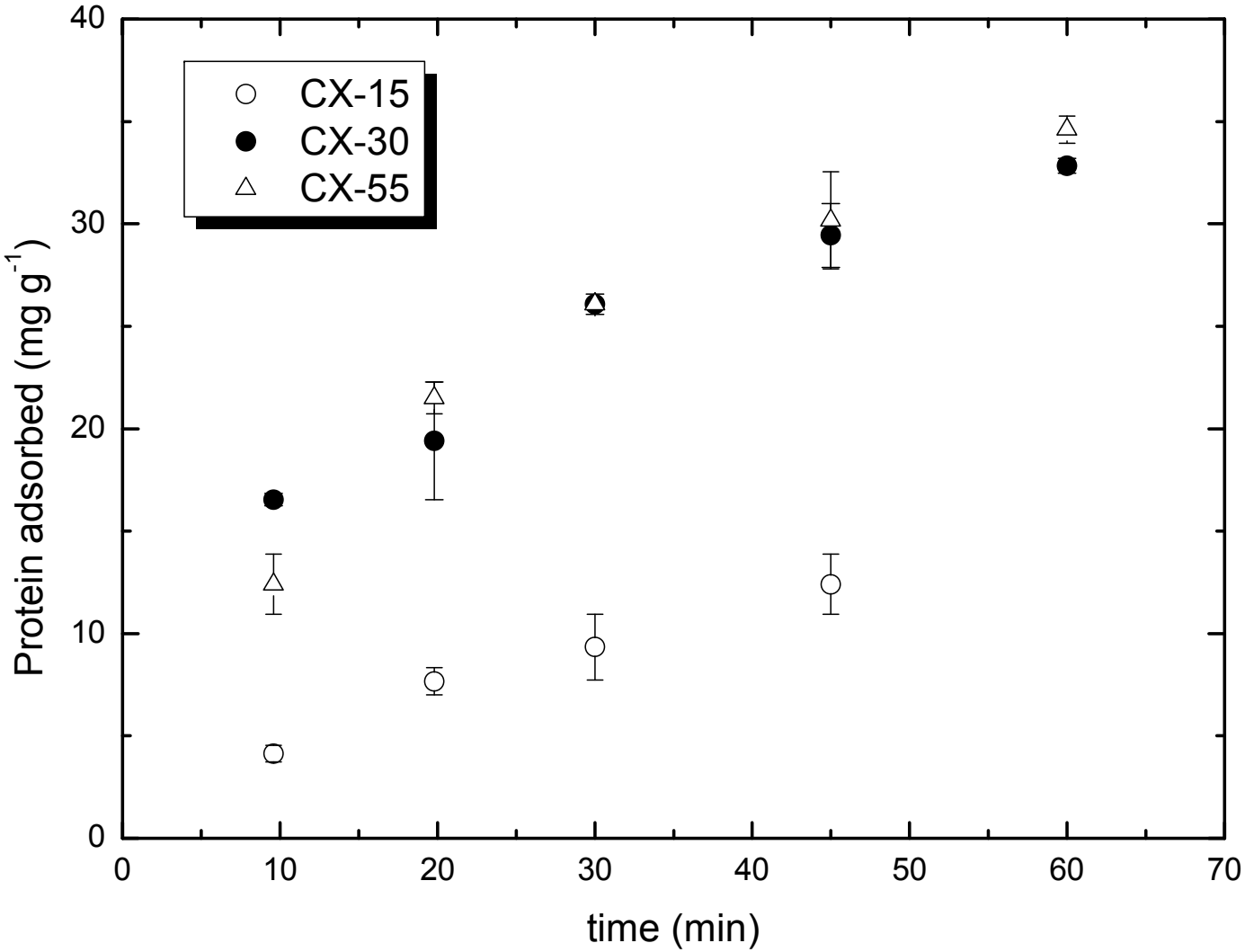

FIGURE S7. Curve fitting of the kinetic experimental results of Figure 6: a) homogeneous diffusion model (eq. 2); b) parabolic diffusion model (eq. 3)

a)

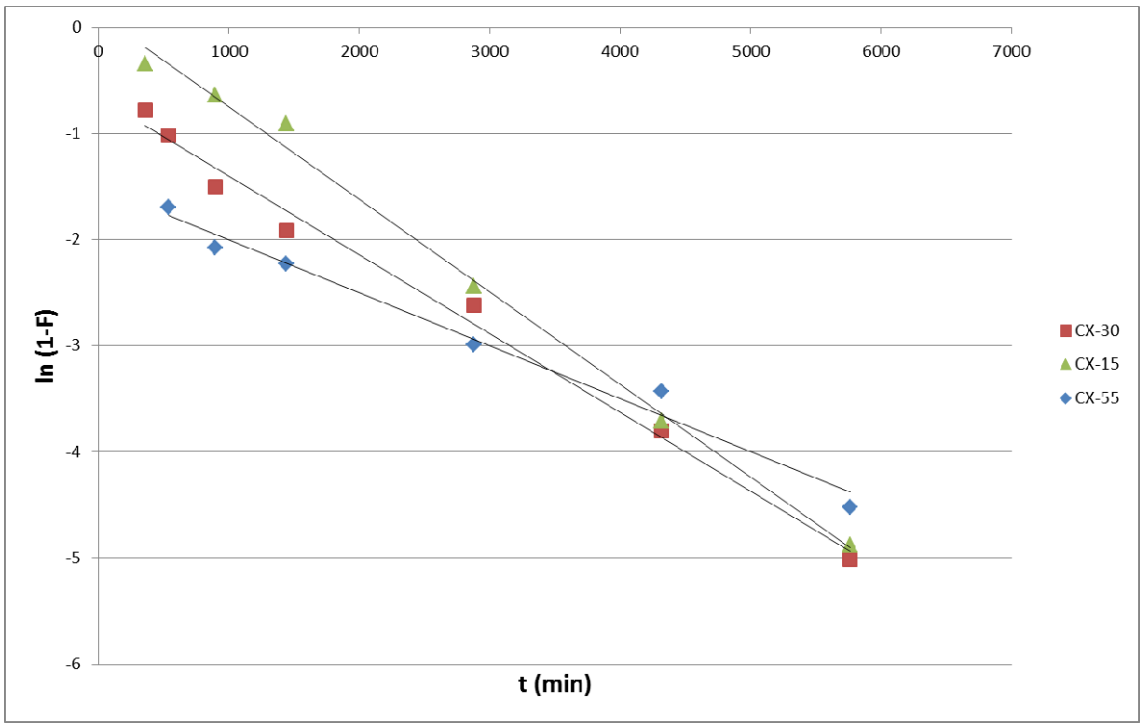

b)

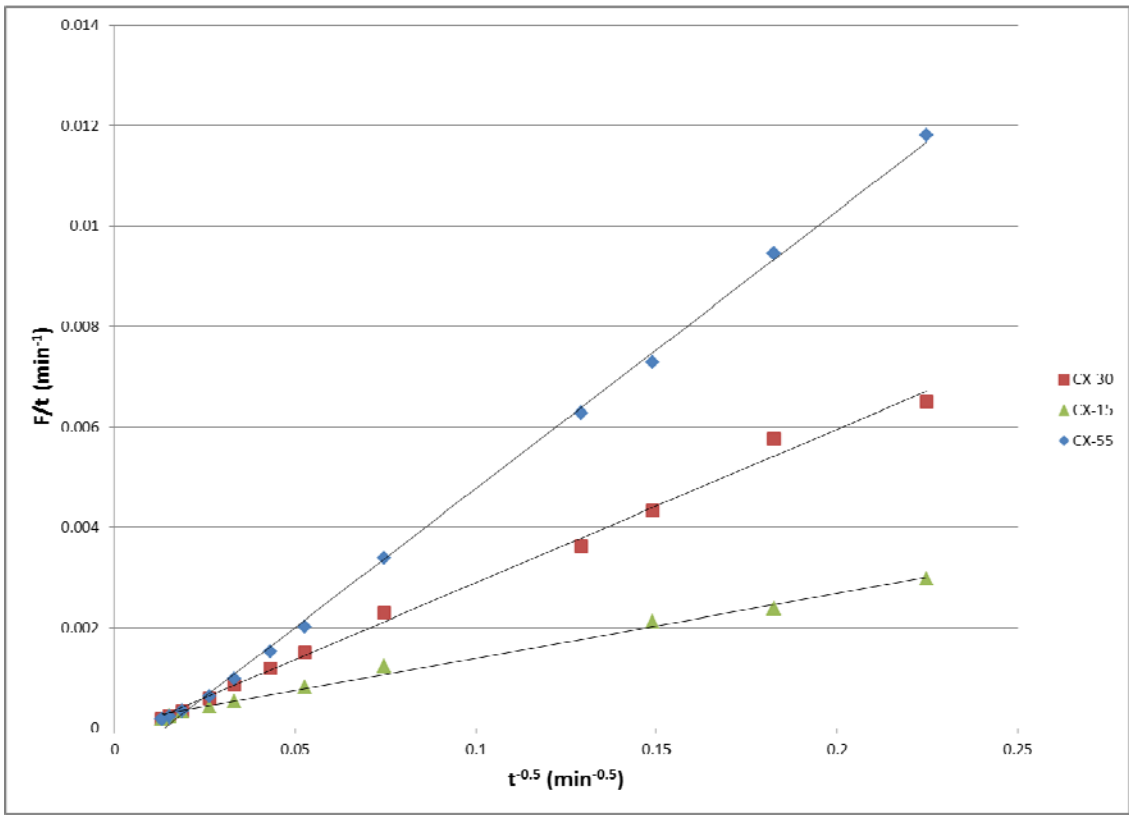

FIGURE S8. Activity (expressed as relative activity; 100 % relative activity corresponds to 1.2 Units per mg cyt c) of 0.5 g L^{-1} cyt c solutions at 30 ºC buffered at [a] three different pH (100 mM). The activity tests were carried out at different pH, as specified in the x axis of the graph.

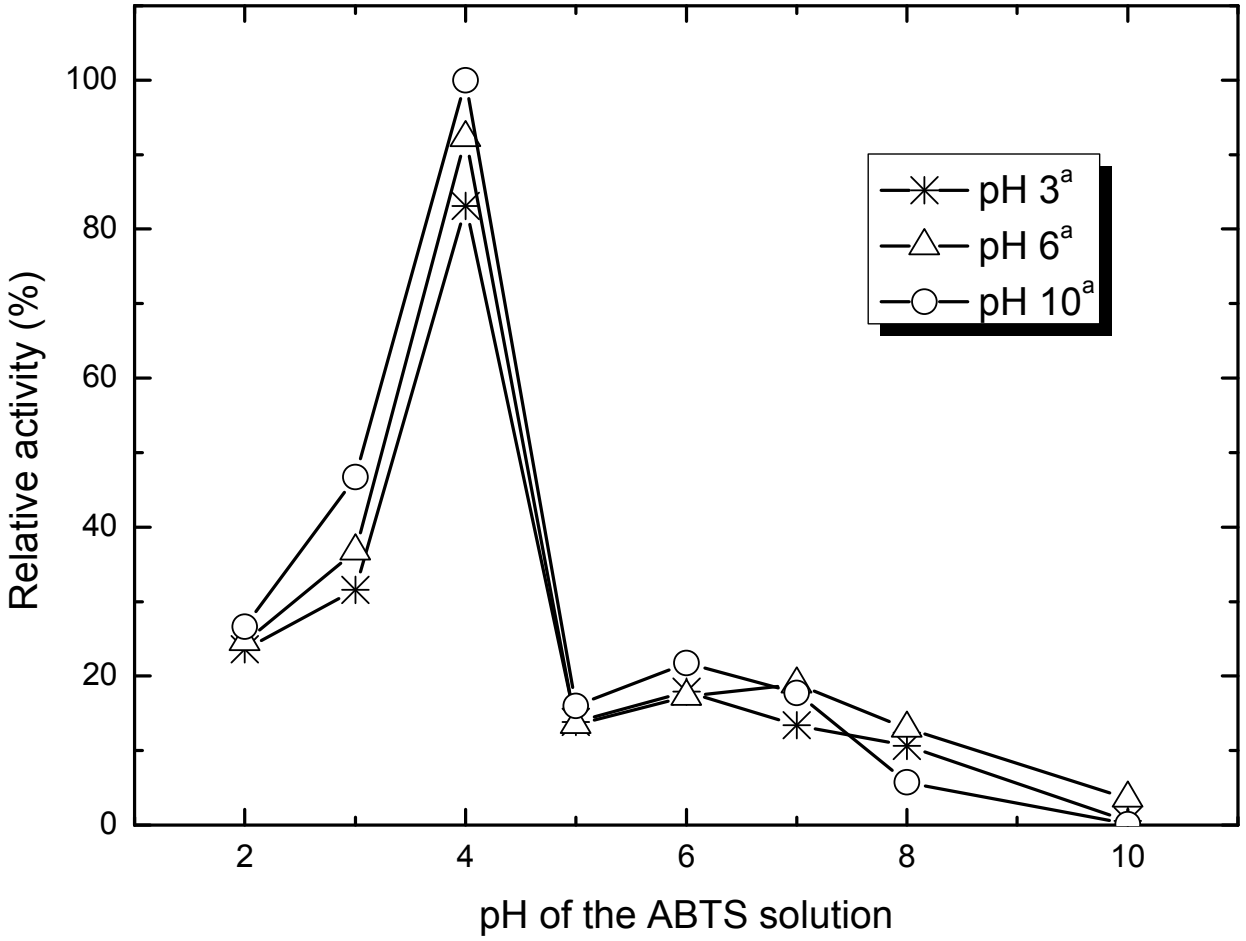

FIGURE S9. Same as Figure 7, but activities expressed in Units per mg of cyt c.